Engineered Neurotrophin-Binding Spider Silk Biomaterials for Nerve Growth Applications

By

Elizabeth A. Baker

Submitted in partial fulfilment of the requirements

for the degree of Master of Science

at

Dalhousie University

Halifax, Nova Scotia

July, 2021

Dedication

To my parents,
for their continued support throughout my never-ending academic journey

To my brothers and sister (in law),
for your company, understanding, and advice

And lastly,

To my small but mighty co-author, Tchai,
for showing me that sometimes the smallest things can make the biggest difference.

Table of Contents

List of Tables

List of Figures

Abstract

Spinal cord injury (SCI) is often accompanied by a lifetime of physical and psychological burden due to the limited capacity for nerve regeneration following development. Spider silks show potential as biomaterials due to their robust mechanical properties and low immunogenicity. Spiders produce up to 7 types of silk, with the toughest being aciniform silk used to wrap prey. Previous work developing production and processing methods of recombinant aciniform silk, including fusion protein constructs, makes the rational modification of this silk to enhance neuronal growth feasible. This thesis describes the production and characterization of a recombinant aciniform silk construct, N_BSilk, functionalized with domains capable of tethering the neurotrophic factor, nerve growth factor-β (NGF-β). N_BSilk films are shown to sequester NGF-β and support the survival, differentiation, and neurite outgrowth of PC12 cells. These results warrant future study of N_BSilk to determine its potential for nerve regeneration applications.

List of Abbreviations Used

AcSp: Aciniform silk spidroins

A. trifasciata: Argiope trifasciata

AKT: Protein kinase B

ATP: Adenosine triphosphate

CNS: Central Nervous System

Col I: Collagen I

Col IV: Collagen IV

dH_2O: Distilled water

E. Coli: Escherichia coli

ELISA: Enzyme-linked immunosorbent assay

ERK1/2: extracellular signal-related kinases 1/2

EtOH: Ethanol

FTIR: Fourier-transform infrared spectroscopy

H_6: Hexahistidine

HFIP: 1,1,1,3,3,3-hexafluoro-2-propanol

HRP: Horseradish peroxidase

IPTG: Isopropyl β-D-1-thiogalactopyranoside

kDa: Kilodalton

MA: Major ampullate silk

MAPK: Mitogen-activated protein kinase

MaSp: Major ampullate spidroin

mTOR: mechanistic target of rapamycin

N_BSilk: Neurotrophin-binding silk

NGF: Nerve growth factor-β

NGF-L: Preloaded with NGF

NGF-M: NGF in cell culture medium

Ni-NTA: Nickel nitrilotriacetic acid

pAKT: phospho-protein kinase B

PBS: Phosphate Buffered Saline

PBST: Phosphate-buffered saline with 0.1% Tween

pERK1/2: phospho-extracellular signal-related kinases

PNS: Peripheral Nervous System

PNI: Peripheral Nerve Injury

SCI: Spinal Cord Injury

SDS-PAGE: Sodium dodecyl sulphate–polyacrylamide gel electrophoresis

R.L.U: Relative luminescence Units

TBST: Tris-buffered saline with 0.1% Tween

TFA: Trifluoroacetic acid

TFE: 2,2,2-Trifluoroethanol

W: Repetitive domain in recombinant aciniform silk

W/v: weight/volume

Acknowledgements

I want to first acknowledge the privilege that it has been to be a member of not one, but two, wonderful academic labs. I've had double the amount of learning experiences, academic support, and fun, that most graduate students encounter during their degree. For providing such positive environments, I want to thank Dr. Jan Rainey and Dr. John Frampton for welcoming me into their lab groups. Both Dr. Rainey and Dr. Frampton have been exemplary role models for me during my time in their labs. Their guidance and feedback has allowed me to grow exponentially as a student. They allowed me to pursue this project with respect to my personal interests and helped me to become more independent and resilient. They have also made it possible for me to pursue this degree, while also working towards my future goals in medicine.

The trials and tribulations of graduate school would not have been possible to overcome without the constant support of my peers and lab mates. Thank you to Dr. Lingling Xu for not only designing the protein at the core of this project, but for all of the training, support, and advice provided to me at the beginning of my degree. Without Lingling, none of this work would have been possible and I can only imagine what more I could have achieved if I had her guidance for the remainder of my research. Thank you also to the Liu Lab for allowing me to use their space and equipment.

Next, I want to extend my gratitude to the amazing PhD candidates in the Rainey lab, especially Jeff and Tam, who were always available to answer my questions when I encountered difficulties. I also want to specifically acknowledge Zachary Visser from the Frampton lab. We started our degrees together, working on similar projects and having similar goals. Zach has been an incredible support to me and I will always appreciate his

ability to listen, understand, and willingly extend compassion. The medical community is lucky to have him!

I would like to give further thanks to my committee members, Dr. Bearne and Dr. Karten for all their guidance during our meetings, as well as Dr. Langelaan and Dr. Ewart for their roles as readers as part of my thesis defence. A warm thanks must also be given to the amazing Roisin McDevitt for her assistance with all the administrative aspects of graduate school, as well as all of her kindness and support regarding my future at Dal. Lastly, thank you to the Canadian Institute of Health Research for providing me with a CGS-M award, and Research Nova Scotia for providing me with a Scotia Scholar's award, both of which greatly helped to support my graduate work.

Chapter 1 :Introduction

1.1: Nerve Injury

Nerves are clusters of fibres that enable communication to be signaled from the central nervous system (CNS) or the peripheral nervous system (PNS) to the rest of the body. Nerves have specialized structural features that allow them to extend over long distances and facilitate this communication. Namely, axons are the specific structural feature of neurons that connect the nerve cell body to other cells to transmit information (Cantile and Youssef, 2016). The blockage or rupture of axons thus inhibits the ability to carry out this communication. Injuries to nerves can occur in both the PNS and the CNS. Due to the limited plasticity of these systems, injuries to either the PNS or CNS can lead to lifelong physical impairment and recovered functionality rarely compares to that of pre-injury (Ahuja *et al.,* 2017). Nerves can be damaged in a number of ways, including by mechanical means, by being partially or completely severed, crushed, compressed or stretched, as well as by pathological mechanisms (Richner *et al.,* 2014). The different nature of each individual injury adds to the complexity of finding successful treatments. Many other factors such as nerve morphology, inhibitory molecules, and scar tissue all contribute to the difficulty of regeneration (Abe and Cavalli, 2008).

Traumatic nerve injuries are the most common occurrence and it is widely accepted in the field that traumatic injuries in the PNS have a much greater capability to regenerate than those in the CNS. Furthermore, the majority of these incidents are seen in adults and the innate regenerative capabilities, especially that of the CNS, decrease drastically with age (Ahuja *et al,,* 2017). The inherent physiological features of the CNS are what limit its ability for regeneration following injury. These features will be

discussed and contrasted with the physiology and pathophysiology of the PNS and PNS injuries to explore the mechanisms and discrepancies in our current understanding of nerve regeneration.

1.1.1: Peripheral Nerve Injury

Peripheral nerve injuries (PNIs) are relatively common, occurring in up to 5% of trauma patients (Althagafi and Nadi, 2021). The pathophysiology of these injuries has been well documented and understood for decades, as well as the molecular mechanisms necessary for regeneration. This is in contrast with CNS injuries, with this disparity likely being due to the fact that PNS injuries are much more common than those of the CNS, as the PNS has less protection from other structures in the body. For example, the CNS is largely protected by a layer of bone such as with the cranium and spine (Cantile and Youssef, 2016). Outcomes for PNIs remain significantly better than injuries to the CNS, but even in this context successful treatment options remain scarce (Caillaud *et al.,* 2018). The outcomes depend on the type of neuropathy, which have been classified into a grading system of 3, by Seddon (1943), which is shown for reference in Figure 1.1

Grade 1 PNI is referred to as neurapraxia and is the least severe type of injury. This is due to nerve continuity not being fully lost, so any motor or sensory impairment can be regained over time (Lee and Wolfe, 2000). Initial functional loss has been attributed to damage to the myelin sheath, which is crucial for electrical conduction. Schwann cells are recruited and assist with the process of remyelination, and, over time, the conduction blockade is resolved (Burnett and Zager, 2004). Grade 2 injuries, known as axonotmesis, involve complete axonal disruption typically due to compressive injury, but the connective tissue remains intact. Grade 3 injuries are called neurotmesis, which

also results in complete axonal disruption, but also include additional disruption of surrounding connective tissues (Lee and Wolfe, 2000). Although grade 2 and 3 injuries are similar, the ability for axons to regenerate is facilitated by the remaining connective tissue structures in grade 2 injuries. The ability for nerves to recover from grade 3 injuries depend largely on the length of gap at the injury site and level of fibrosis that occurs. More often than not, surgical intervention is required with grade 3 PNI to facilitate bridging the gap at the injury site (Campbell, 2008).

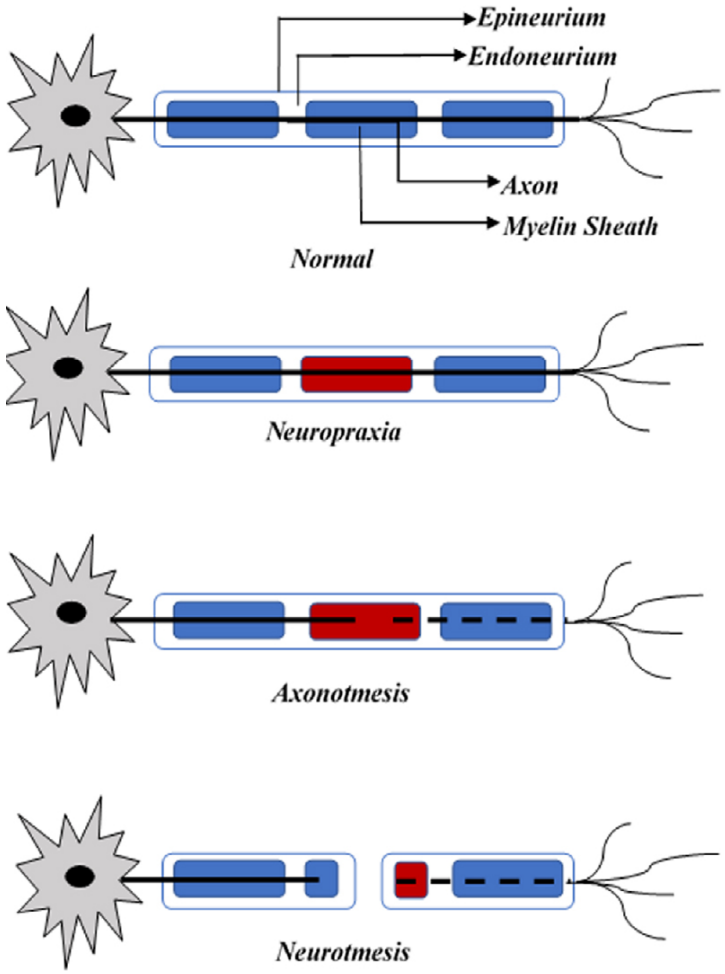

Figure 1.1: Seddon's Classification System for Peripheral Nerve Injuries. The top of the image shows a schematic representing a healthy nerve and its key anatomical features, followed underneath by each grade of PNI in order from 1-3. Image from Chandrasekaran et al., (2020), used with permission from Wolters Kluwer Medknow Publications.

1.1.2: Wallerian Degeneration

The latter two grades of PNI result in the critically important process of Wallerian degeneration (WD), initially described by Waller and Owen, (1850). WD is a phenomenon initiated by Schwann cells at the site of injury to clear debris from the axonal distal stump. This is the first step in achieving nerve regeneration, as efficient WD has been linked to improved functional recovery following PNI (Rotshenker, 2011). During this process, Schwann cells clear any myelin debris via phagocytosis and recruit inflammatory immune cells both chemotactically and cytotactically to assist with clearing axonal debris (Burnett and Zager, 2004). The process of WD begins hours after injury and takes between 5-8 weeks to complete. It is at this point that regenerative processes can begin (Weinburg and Spencer, 1978). For a schematic representation of the WD process, refer to Figure 1.2.

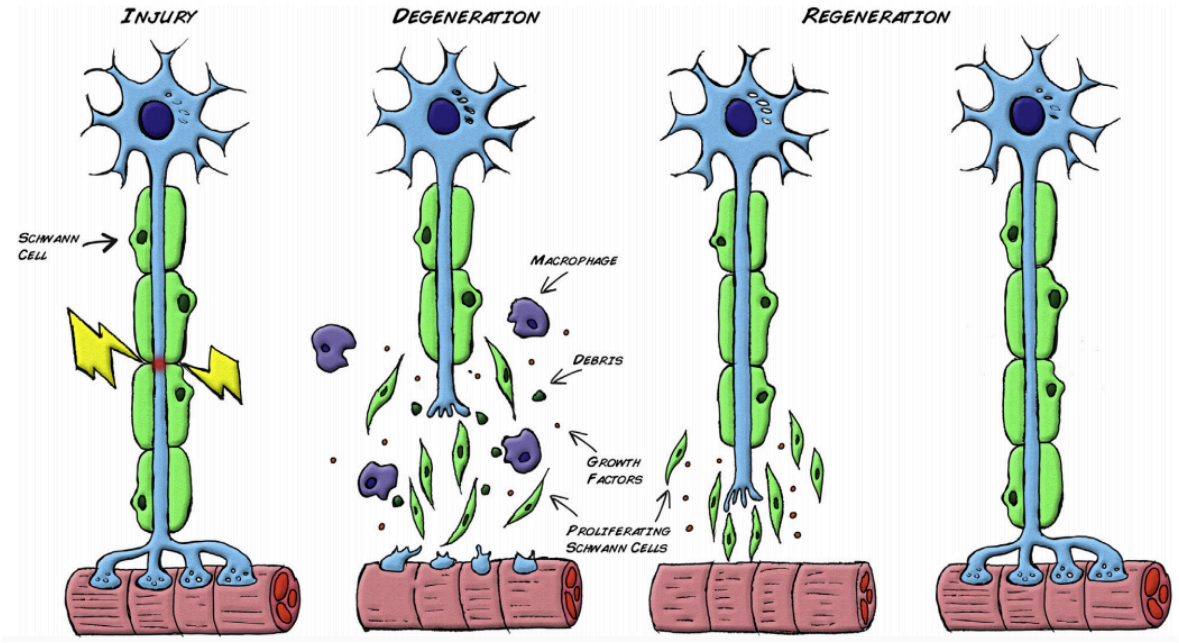

Figure 1.2: Schwann Cell-Mediated Wallerian Degeneration in the PNS Following Injury. Reused from Feroni et al., (2015), with permission from Elsevier.

Schwann cells are one of the main contributors of nerve regeneration in the PNS. Not only do they initiate WD, but in the first day following injury they become altered phenotypically by upregulating molecules critical for WD and regenerative processes (Burnett and Zager, 2004). Adhesion molecules like neural cell adhesion molecule (NCAM) and L1-CAM are expressed to create a more favourable environment for axonal extension (Kiryushko *et al,* 2004). The expression of growth factors including nerve growth factor (NGF), among others, is also upregulated to stimulate cell survival, proliferation, and axon growth. During this period of phenotypic shift, Schwann cells also align into columns, called bands of Bünger. The secretion of neurotrophic factors in this specific environment collectively allow nerve regeneration of the PNS (Richner *et al.,* 2014).

1.1.3: Spinal Cord Injury

As part of the CNS, injuries to the spinal cord are a traumatic event that often result in permanent disruption of sensory, motor, and autonomic function. The lack of regenerative capacity of the CNS has a large impact on a patient's quality of life following injury. Not only do these injuries impact physical well-being, but they also lead to psychological, social, and economical burden to patients, families, and the healthcare system (Singh *et al.,* 2014). It is difficult to achieve the regeneration of damaged nerves in the CNS due to the lack of stimulatory growth factors in adults. Furthermore, the blood-brain and -spinal cord barriers are critical for maintaining homeostasis in the CNS. Injury to these barriers results in the influx of inflammatory cells and inhibitory molecules (Abe and Cavalli, 2008).

In general, neurons of the CNS do not upregulate growth factors after development. Therefore, intrinsic ability for regeneration is limited (Ahuja *et al.,* 2017). Oligodendrocytes are known as the Schwann cells of the CNS, as they provide the insulating myelin sheath which is essential for axon extension and signal conduction (Yiu and He, 2006). Due to oligodendrocyte apoptosis and the lack of debris clearance, a build-up of scar tissue often occurs at the site of injury. This glial scar tissue prevents the growth of nerves through both a physical blockage for axon extension, as well as inhibiting the recruitment of necessary stimulatory cells to support neuron survival (Chen *et al.,* 2007). Microglia are known as the macrophages of the CNS. Following spinal cord injury they have been observed to swiftly proliferate to initiate a robust inflammatory response. The influx of these cells to the site of injury in the spinal cord also creates an unfavourable environment for cell growth (Cantile and Youssef, 2016). In fact, the disruption of proper microglial function now serves as a main hypothesis for driving neurodegenerative diseases such as Alzheimer's disease and Parkinson's disease (Wong, 2013; Sierra *et al.* 2014). For decades it has been proven that the surrounding environment is critical for nerve regeneration in the CNS. Foundational work has shown how axons that were otherwise unable to grow, were able to extend over long distances by using peripheral nerve grafts to create a more permissible environment (Huebner and Strittmatter, 2009).

1.1.4: Current Therapeutic Strategies

Early intervention is critical for treating nerve injuries. Immobilization of the spinal cord is necessary immediately to prevent any further damage. Surgical decompression is often key to limiting further injury by increasing blood supply to the

affected area (Ahuja *et al.,* 2017; Batchelor *et al.,* 2013). Other than surgical intervention, there are some pharmacological treatments currently used as standards of care, and many others being researched. Those currently used include steroids to reduce inflammation and oxidative stress, ion channel blockers to protect against unregulated excitatory activity that contributes to cell death, and antibiotics to protect against infection from injury (Bracken, 2012; Azbill and Springer, 2000). Some antibiotics such as minocycline have also been found to exhibit potent anti-inflammatory effects by suppressing microglial activity (Ahuja *et al,* 2017).

The adult mammalian CNS expresses many inhibitory molecules, such as myelin-associated inhibitors and neurite outgrowth inhibitor A (NOGO) , which limit axon growth and contribute to difficulties in nerve regeneration following injury (Abe and Cavalli, 2008). Interestingly, fish, which are our distant vertebrate relatives, have a much greater capacity for nerve regeneration, but many of the regulatory pathways involved in axonal outgrowth remain conserved (Rasmussen and Sagasti, 2017). It is hypothesized that functional divergence has occurred amongst the conserved inhibitory molecules, which results in the greater ability for fish to overcome inhibitory cues and ultimately achieve recovery following injury (Shypitsyna *et al.,* 2011). Additionally, factors that block inhibition and the upregulation of pro-growth factors have been proposed as other explanations for the intrinsic ability of fish to achieve functional nerve repair (Rasmussen and Sagasti, 2017; Kato *et al.,* 2013). Current advancements in treating mammalian CNS injuries, which will be discussed next, have used the information gathered from fish model systems to better target the molecular mechanisms involved in axon repair.

Clinical trials for novel pharmacological treatments are currently underway targeting specific inhibitory molecules that have been discovered in the spinal cord following injury. NOGO as well as myelin-associated proteins and glycoproteins, bind to specific receptors to activate Rho A GTPase. Subsequent signalling activates the effector molecule, Rho-associated protein kinase (ROCK), which ultimately induces inhibition of the axonal growth cone, resulting in neurite retraction or even apoptosis (Cafferty *et al.,* 2010). As this signal transduction cascade has been implemented in halting regeneration, it has been one of the main starting points for inhibitory molecule and monoclonal antibody therapeutics for spinal cord injuries. Rho-Rock inhibitors are currently in phase III clinical trials and Anti-NOGO therapies have just finished phase I clinical trials pending dissemination, results of initial studies with these inhibitors have shown promising results and are moving forward with more trials (Fehlings *et al.,* 2011; Ahuja *et al.,* 2017).

1.1.5: Biomaterial Approaches as Novel Treatments

In addition to molecular mechanisms, the physical obstruction of scar tissue remains a key obstacle for nerve regeneration (Chen *et al.,* 2007). To simultaneously address these issues, biomaterial therapies have emerged as promising strategies. Biomaterials in the form of nerve guidance conduits have, for example, been a main focus to help guide the growth of axons by bridging the gap at the site of injury (Fine *et al.,* 2001).

Nerve guidance conduits made from biomaterials address many of the issues associated with current standards of care for PNI, such as the nerve autograft. For this treatment a piece of healthy nerve tissue is taken from a donor site on the body and

implanted into the injury gap. Nerve grafts require availability of donor tissue, more extensive surgery, and lead to a loss of sensation at the donor site. Furthermore, these surgeries are not always successful and patients are left with additional recovery (Evans *et al.,* 1998). Biomaterial scaffolds and guidance conduits may be able to address these limitations, which will be discussed next.

To date, guidance conduits have been engineered to mimic the extracellular matrix (ECM), release appropriate growth factors, or even be seeded with stem cells. Guidance conduits can be made of natural or synthetic materials to mimic a permissible environment for nerve regeneration (Tam *et al.,* 2012). Although this sounds promising for treatment, clinical trials with PNS nerve guidance conduits, including those that are now commercially available, have not been able to achieve the same degree of functional recovery compared to the standard of care autograft. To put that into perspective, PNS nerve autografts typically only increase the chances of functional recovery by 50 % (Song *et al.,* 2020). Most current biomaterials approved by the FDA and on the market are collagen-based scaffolds, but have been found to only be suitable for PNIs $\leq$ 3 cm in length (Kehoe *et al.,* 2012; Carvalho *et al.,* 2019).

The success of guidance conduits for PNI, albeit limited, has encouraged the development of biomaterial therapies for spinal cord injuries. Physiological differences between the PNS and CNS require distinct considerations for engineering appropriate materials for the spinal cord (Straley *et al.,* 2010). Critical design elements involve the promotion of cellular adhesion, physical guidance cues, mechanical strength, biodegradability and the delivery of neurotrophic factors.

1.2: Silk Proteins

Silks are natural materials that are spun by animals for a variety of purposes and which have been harvested by humans for textile and medical applications since ancient times (Holland *et al.,* 2012). Animals that produce silks include spiders, silkworms, bees, and wasps, to name a few. Silks are composed of proteins that assemble to produce fibres. The types of protein formed into a silk depends on the organism, with some organisms producing multiple types of silk proteins and silks, with species-specific differences (Sutherland *et al.,* 2012). Spiders, for example, can produce up to 7 different types of silk proteins - or spidroins (Figure 1.3) - with unique biological functions, while silkworms produce only one, silk fribroin. Silks have evolved over time to better the survival of these animals by helping with protection, shelter, capturing prey, and withstanding environmental pressures (Lewis, 2006). Thus, silks display robust mechanical properties, yet are biodegradable, which makes them of interest for material applications.

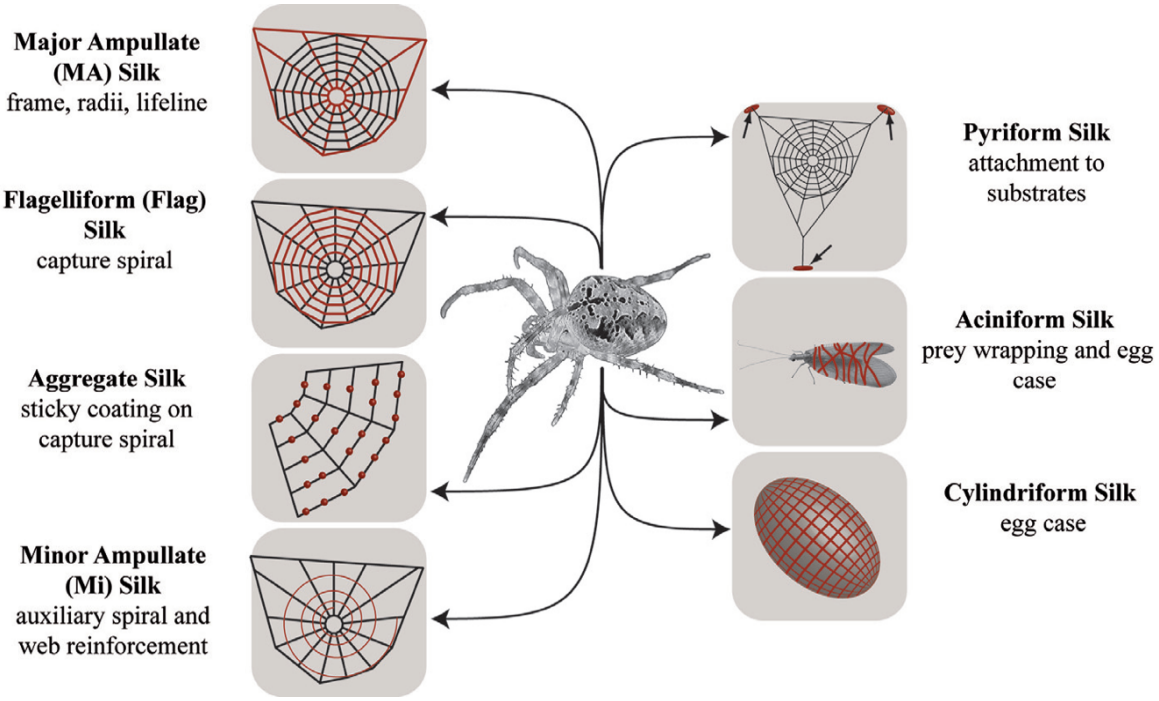

Figure 1.3: The Types of Spider Silk. Reproduced from Eisoldt et al., (2011), with permission from Elsevier.

1.2.1: Spider Silk

The different biological functions of spider silks noted above (Figure 1.3) are correlated with unique structural and mechanical properties. In nature, their different features allow for the production of the most advantageous web for the spider. Spider dragline silk is mechanically the strongest of all 7 types. It is made up of major ampullate proteins, MaSp1 and MaSp2 in *Nephila clavipes,* and ADF-3 and ADF-4 in *Araneus diadematus,* which collectively have been the most widely studied spidroins to date. This type of silk is a critical structural component of the spider web, as it composes the frame (Borkner *et al.,* 2014; Eisoldt *et al.,* 2011). Minor ampullate silk is an element of the web spiral, used as reinforcement. Flagelliform silk acts as the interior structure of the web in the capture spiral, which is further coated by aggregate silk to enhance prey capture (Hayashi and Lewis, 1998). Pyriform silk is similarly sticky to aggregate silk, but instead

of prey capture, it allows the spider to attach the web to substrates (Simmons *et al.,* 2019). Cylindriform silk encases spider eggs to protect offspring and aciniform silk offers further structural integrity to the inner casing of eggs. Aciniform silk is also used in a second context to wrap the spider's prey (Eisoldt *et al.,* 2011). The distinct mechanical properties of each spidroin allows for the rational selection based on these properties when studying or using silks for material applications, such as the toughness of aciniform silk, which will be specifically employed herein, so will be discussed in more depth next.

1.2.2: Aciniform Silk

To withstand the forces involved with successfully restraining live prey, aciniform silk is the toughest of the spider silks described in section 1.2.1. Toughness refers to the material's ability to be both strong and extensible. Aciniform silk is comprised mainly of the protein, aciniform spidroin 1 (AcSp1), which has been studied through protein sequencing in a variety of species (Hayashi *et al.,* 2004). This protein ranges from 300-430 kDa, depending on the species, and is comprised of highly conserved repetitive units, separated by short non-repetitive linkers, and non-repetitive N- and C-terminal domains. In *Argiope trifasciata* there are 14 of the 200 amino acid long repetitive sequences (Hayashi *et al.,* 2004).

The secondary structure of spidroins is what determines the mechanical properties of their silk fibres. A combination of β-sheets with amorphous and α-helical regions allow both the tensile strength and extensibility observed in aciniform fibres. The β-sheet regions provide a highly aligned and compact structure that contributes to rigidity needed for strength, while the amorphous regions and α-helicity allow for more plasticity (Nova *et al.,* 2010).

1.2.3: Recombinant Spider Silks

It is currently understood that for producing silk at a large-scale, which is necessary for material applications, harvesting through sericulture is not a viable option. This is due to the cannibalistic nature of spiders, as well as the finding that the quality of silks spiders produce when held in captivity tends to be inferior and inconsistent. It is also difficult to collect and isolate the individual types of silks from spider webs (Borkner *et al.,* 2014; Heidebrecht and Schiebel, 2013). To avoid these challenges alongside the resulting variability in protein quality, methods to produce and process recombinant silk proteins have been pursued. As a further benefit with respect to harvesting natural silks, it is possible to alter and tailor the protein sequence when engineering recombinant silk constructs (Borkner *et al.,* 2014).

Recombinant aciniform silks have previously been successfully expressed in *Escherichia coli* and cast into films or spun into fibres in our lab. These aciniform constructs are modelled after the AcSp1 protein from *A. trifasciata,* with sequence and mechanical properties as first reported by Hayashi *et al.,* (2004). The structure of AcSp1 is shown in Figure 1.4. The recombinant proteins are comprised of 1 to 4 repetitive "W" (from wrapping silk) units within the core domain. Therefore, these constructs are much smaller than native proteins, but more feasible to express recombinantly. The protein constructs require 2 or more "W" units to achieve the necessary interlocking for fibre formation (Xu *et al.,* 2012a). As the proteins are much smaller than those in nature, the mechanical properties of recombinant aciniform fibres do not parallel natural silks; however, they still exhibit both strength and extensibility. Additionally, the study of

different fusion constructs and post-spin stretching treatments have assisted with enhancing these mechanical properties (Xu *et al.,* 2017; Xu *et al.,* 2019).

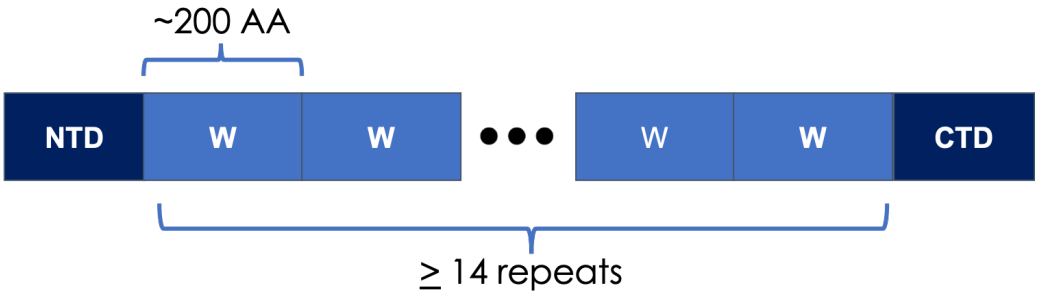

Figure 1.4: Structure of Recombinant Aciniform Silk. Based on the AcSp1 protein from Argiope trifasciata as described by Hayashi et al., (2004).

1.3: The Present Work: Engineering Rationally-Designed Recombinant Spider Silk

Spider silks are an outstanding option for biomaterials. Their mechanical properties combined with their biocompatibility and tunability make them highly desirable for medical applications (Leal-Egaña and Scheibel, 2010; Salehi *et al.,* 2021; Kiselva *et al.,* 2021). For example, silk fibres have been explored for sutures, wound dressings, artificial tendons or ligaments, and silk films have been studied for device coatings with antibacterial, cell adhesion, drug delivery, and other properties. Silk has also been formed into sponges and hydrogels to act as scaffolds or to fill various defects following surgery or injury (Baoyong *et al.,* 2010; Hennecke *et al.,* 2013).

Recombinant silk proteins have been successfully expressed and purified, which allows for the rational modification of their protein sequences for specific applications. The desired application for this work is to develop a biomaterial to support the survival of nerves and promote neuritogenesis, or the sprouting of neurites, which is a determining factor of regeneration following injury. A novel recombinant aciniform silk construct was

bioengineered to attract the neurotrophic factor, NGF, to enhance neuronal growth and survival. The role of NGF in nerve regeneration is discussed in the following sections.

1.3.1: Nerve Growth Factor Signaling

Binding motifs for the neurotrophic factor, NGF, were selected as part of the engineering of a recombinant aciniform silk construct due to its critical role in nerve growth and survival. One of the most likely determinants of neuronal death and lack of regeneration following injury is the withdrawal of neurotrophic support (Fricker *et al.,* 2018). As discussed in section 1.1.3, the formation of glial scar tissue, as well as the lack of cell survival signals in the spinal cord after injury, lead to cell apoptosis which thereby halts necessary regenerative cellular mechanisms, such as the upregulation of growth factors. The discovery that NGF was present in the distal and proximal stumps following rat spinal cord transection studies further led to the hypothesis that this neurotrophin is critical for axon extension and subsequent nerve injury repair (Murakami and Furukawa, 2002).

NGF elicits growth, differentiation, and survival signaling to cells by binding primarily to its high-affinity receptor, tyrosine kinase A receptor, or TrkA. There is another low-affinity receptor called p75 non-tyrosine kinase receptor, or $p75^{NTR}$. The main neurotrophic actions of NGF are signalled through TrkA, while $p75^{NTR}$ helps to regulate these effects by actually signaling apoptosis, thus prohibiting the over stimulation of growth and survival signals that could cause deleterious effects on cells (Bibel *et al.,* 1999).

Following NGF binding to TrkA, two main signal transduction cascades follow which are shown for reference in Figure 1.5. The mitogen activated protein kinase

(MAPK) pathway is a well-studied target of TrkA activation by NGF. The autophosphorylation of TrkA following the binding of NGF signals the recruitment of various adaptor proteins and complexes such as SHC, GAB1, and GRB2, which collectively allow SOS to interact with the membrane-associated Ras. This stimulates a kinase phosphorylation cascade via Raf. The downstream phosphorylation targets, extracellular signal-related kinases 1 and 2 (ERK1/2), are then able to translocate to the nuclease to activate pro-survival and differentiation genes (Kim *et al.,* 2004; Klesse *et al.,* 1999; Terada *et al.,* 2014).

Additionally, TrkA activates phosphatidylinositol-3 kinase (PI3K) and allows for recruitment of AKT from the cytosol to the plasma membrane. AKT is then dually phosphorylated and can activate p21-activated kinase 1 (PAK1) (Higuchi *et al.,* 2003). Although not all of the mechanisms for how the PAK1 pathway stimulates axon extension are understood, it has been observed that PAK1 modulates cell motility and may contribute to scaffolding via actin rearrangement to promote neurite outgrowth (Higuchi *et al.,* 2008). Furthermore, it has been shown that AKT inhibitors prevent PAK1 phosphorylation and neurite outgrowth in PC12 cells (Park *et al.,* 2020). AKT is also present at the tips of growth cones and has been implicated in axon elongation and suppression of axon branching (Higuchi *et al.* 2003). Both of these findings provide evidence for the role of AKT in neurite outgrowth. AKT activation can also lead to a number of downstream effects that contribute to cell survival, such as the activation of the mechanistic target of rapamycin (mTOR), to

promote cell proliferation and survival through transcription of growth factors (Xu *et al.,* 2020).

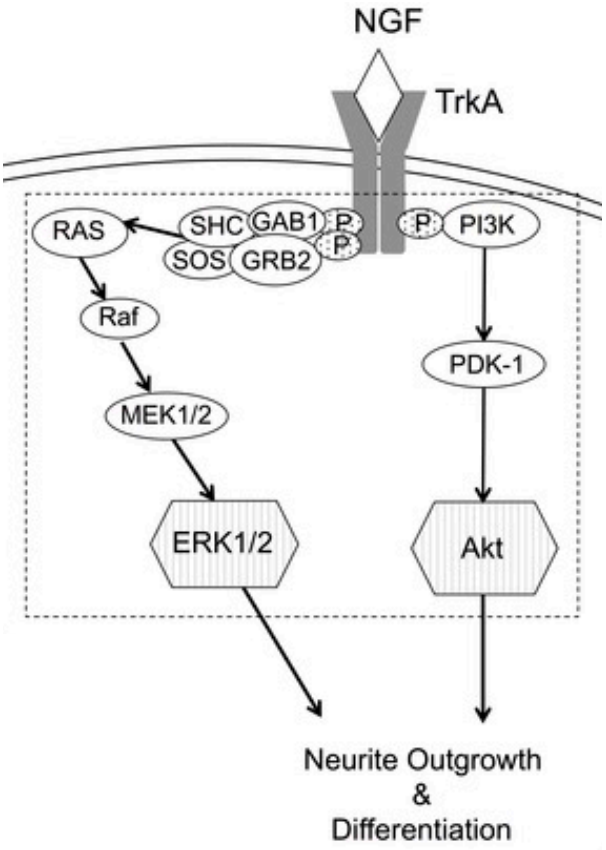

Figure 1.5: NGF Signaling Pathways through MAPK and PI3K. NGF binding signals the autophosphorylation of TrkA, which recruits adaptor proteins SHC, Gab1, and GRB2. This allows the proximity of SOS to Ras which activates Raf to initiate a series of kinases known as MEK. Downstream phosphorylation of ERK1/2 allows the nuclear translocation to activate differentiation-related transcription factors. NGF can also activate PI3K which results in downstream phosphorylation of AKT by PDK-1 to enhance transcription of pro-survival genes and allow for the arrangement of scaffolding molecules necessary for neurite outgrowth. Edited from: © Terada et al., (2014), Used with permission under the terms of the Creative Commons Attribution License: CC BY 4.0.

NGF is produced by non-neuronal cells during development to assist with the extension of neural projections to target sites. In neuronal cells of the PNS, like Schwann cells, NGF is upregulated during development, but expression is greatly downregulated once maturity of myelinating cells is achieved (Mirsky and Jesson, 1999). NGF production continues into adulthood following response to stimuli, such as injury.

Following PNS injury, immune cells stimulate Schwann cells to upregulate NGF expression during the inflammatory response, which creates a positive feedback loop by increasing the amount of myelination occurring for extending nerves, as well as recruiting more Schwann cells to the injury site and triggering the increased expression of TrkA and NGF to continue this cycle (Anton *et al.,* 1994). These cascades contribute to the regenerative ability observed in the PNS. The role of NGF in the CNS is similar to that of the PNS; however the lack of Schwann cells in this system, as well as the frequent apoptosis of oligodendrocytes and formation of scar tissue following injury, limit the expression and or availability of NGF and TrkA (Chen *et al.,* 2007).

1.3.2 Nerve Growth Factor-Based Biomaterials

Researchers have studied NGF -based biomaterials in the past with conflicting results. Initially, materials loaded with NGF were not able to control the growth factor release and NGF leaked or became biologically inactive (Chen *et al.,* 2002). Furthermore, the administration of NGF into the PNS and CNS, including the spinal cord, has caused off-target neurite sprouting which can lead to chronic nerve pain and inappropriate reflex (Krenz *et al.,* 1999). Contrarily, nerve guidance conduits implanted in the rat PNS were able to achieve successful regeneration of the sciatic nerve over long distances (Fine *et al.,* 2002). The application of these materials in clinical settings is still surrounded by hesitation due to previously mentioned negative side effects.

Natural silks have long been a biomaterial of interest for nerve regeneration due to their mechanical properties. Silk fibroin from *Bombyx mori* has been well studied, but was found to produce an inflammatory response *in vivo*, causing a shift in focus to spider silks (Millesi *et al.,* 2021). Dragline silk has been the main silk studied in animal models

and has been able to achieve cell adhesion, alignment, and proliferation in short PNS injury rodent models, as well as longer (6 cm) defects in ovine models (Kornfeld *et al.,* 2021). Unfortunately, limited data exists for models of CNS regeneration, and nerve injury models in general with silks other than dragline. This is likely due to the more difficult nature of CNS regeneration and the wider body of literature pertaining to dragline silk. Therefore, studying novel materials with more favourable mechanical properties (i.e toughness), and producing recombinant variations of these proteins that are engineered in ways to specifically address the limitations of CNS regeneration, is important for finding potential therapeutics.

1.3.3 Project Objectives and Hypotheses

To produce a silk specifically for the application of promoting nerve regeneration, the protein sequence derived from AcSp1 shown above in Figure 1.4 was modified, starting from a previous fusion protein construct produced and characterized by our group (Xu *et al.,* 2017). Namely, the recombinant aciniform silk fusion construct, HW_2C_{Ma2}, was used as the basis for this construct and further modified by the addition of a neurotrophin-binding (N_B) sequence at both termini of the protein. The N_B binding sequence chosen is specific for the neurotrophic factor, NGF, as determined by Okur *et al.,* (2018). A schematic of this protein construct which has been named N_BSilk, for NGF-binding silk, is shown in Figure 1.6.

Figure 1.6: Schematic of N_BSilk. The NGF binding motif added to the N and C-termini of the recombinant aciniform protein is highlighted in yellow. The H_6 tag follows the N-terminal binding motif, shown in orange. The two 200 amino acid repetitive W units from A. trifasciata are shown in blue. Lastly, the C-terminal domain is shown in green.

Aciniform silk is a desirable material for this application due to its combination of mechanical properties. For example, dragline silk is the strongest of all silks, with similar strength to synthetic materials such as Kevlar, but lacks appropriate extensibility. Contrarily, flagelliform silk has high extensibility, comparable to nylon (Hinman *et al.,* 2000). To act as a biomaterial in the human body, which is not static and must withstand forces of movement, stretching, compression, etc., a combination of these mechanical properties is ideal. Aciniform silk addresses this need with high toughness compared to other types of spider silk (Xu *et al.,* 2019). This combination of tensile strength and extensibility make it an appropriate selection for engineering recombinant constructs for biomaterial applications, such as nerve growth substrates or guidance conduits.

The present work aims to investigate the novel recombinant aciniform silk construct, N_BSilk, as a potential biomaterial to address the lack of current successful therapeutic options for those suffering from nerve injuries, specifically those of the spinal cord**.** The overall objectives for this project were to express, purify, and characterize the N_BSilk construct, that has been rationally-designed and bioengineered to sequester the neurotrophic factor, NGF. My goal was to determine appropriate conditions to use N_BSilk for cell culture experiments in order to establish its potential as a scaffold for neural regeneration applications. Through its binding and/or release, I hypothesized that the silk would improve the presentation of NGF to cells to promote their survival when cultured on the silk *in vitro*, as well as stimulate neurite outgrowth, which is a critical first step in regeneration following injury.

Chapter 2 : Neurotrophin-Binding Silk Production and Characterization

2.1: Overview and Experimental Objectives

In Chapter 1, I proposed the application of a recombinant aciniform silk construct designed for nerve tissue engineering and regenerative medicine. Since this is a novel recombinant protein, it was previously unknown if and how this silk could be produced. As such, my first objective was to develop an expression and purification protocol for N_BSilk. Previous research has elucidated mechanisms for the production and fibre wet-spinning of recombinant W_2 proteins, including fusion constructs (Xu *et al.,* 2017). Since W_2C_{ma2} is the core domain of N_BSilk, similar methods, which will be discussed below , could be pursued and modified accordingly. Following protein production, I planned to cast N_BSilk into films and characterize its ability to sequester and release NGF, to determine if it would be an appropriate biomaterial for future cell culture studies.

E. coli as a protein expression system has been the focus of recombinant aciniform silk production in our lab and has been widely used for other types of recombinant spidroin production as well (Huemmerich *et al.,* 2004; Xia *et al.,* 2010; Xu *et al.,* 2012b; Simmons *et al.,* 2019*). E.* coli expression systems are relatively straightforward and popular due to their cost-effectiveness (Rosano and Ceccarelli, 2014). Fibre wet-spinning requires large volumes of concentrated protein solution, so a high expression yield is one of the main requirements of recombinant silk production. For materials applications, the production of silk must also be scalable. This is one of the main motivations to produce artificial silks, as spiders held in captivity tend to produce lower quality and quantities of silks (Heidebrecht and Schiebel, 2013). Previously, our lab has exploited the use of His-SUMO tags in an attempt to increase protein expression

and ease purification (Xu *et al.,* 2012a). The N_BSilk construct does not contain a SUMO tag and the His tag is slightly internal of the N-terminus, as opposed to directly at the terminus of the construct like previous W_2 constructs. Therefore, the purification strategy had to be altered to account for this as is detailed in section 2.2.1.

For fibre wet-spinning, the recombinant silk must be solubilized in a dope solution to facilitate the self-assembly of proteins and subsequent formation of fibres under shear force. This protein solubilization is also necessary for film casting, so the recent discovery of highly effective recombinant aciniform silk dope solvent conditions could be applied to this work (Xu *et al.,* 2019). It is hypothesized that N_BSilk fibres will promote the growth of nerve cells by sequestering NGF to stimulate differentiation and guide cellular outgrowth with their long and narrow structure. However, it is impractical to produce a large quantity of fibres for preliminary cell culture studies without knowing if the protein construct is functional for the proposed application. It is for this reason that the present work will focus on silk films as opposed to fibres. Film production requires less protein than fibre spinning and is easier to scale for more high-throughput biochemical analyses, such as with 96-well plate-format experiments. Additionally, identifying solvents that are appropriate for film casting can be translated to wet-spinning dopes for future fibre production. Lastly, films and coatings are a highly sought-after form of protein-based materials for biomedical applications. Biomaterials can be coated with silk to enhance cellular adhesion, proliferation, and ultimately regeneration for tissue engineering applications, such as in cardiac tissue engineering, as was recently shown by Kramer *et al.,* (2020), using a recombinant dragline silk.

This chapter focuses on the production and characterization of the novel recombinant aciniform silk construct, N_BSilk. Since this construct is based on the previously studied recombinant aciniform silk protein, $HW_2C_{ma2,}$ similar expression and purification protocols were tested and then tailored to enhance the expression of N_BSilk, specifically. Each aciniform construct behaves slightly differently due changes in primary structure, so it was initially unknown if this construct could be expressed at levels suitable for the production of biomaterials, such as films and fibres. My first objective was to optimize the expression and purification of N_BSilk from *E. coli* cells. The second objective was then to test the solubility of N_BSilk in solvents appropriate for both film casting and fibre wet-spinning. Since films were the focus of this research, they were analyzed optically, spectroscopically, and using specifically-developed immunoassay techniques. The following experimental results suggest that N_BSilk has the potential for biomaterial applications. These results allowed me to proceed with using N_BSilk films as a substrate for cell culture, which will be detailed in Chapter 3.

2.2: Materials and Methods

The recombinant protein used for this project will be referred to as N_BSilk. This construct contains NGF-β binding motifs (N_B;sequence:NERALTL determined by Okur *et al.,* 2018) fused to both termini of the recombinant aciniform protein, HW_2C_{ma2}, which consists of a hexahistidine tag (H), 2, 200-amino acid repetitive "W" units of AcSp1 and the CTD of MaSp2 from *Argiope trifasciata*. The sequence of this protein is described in Figure 2.1.

MGNERALTLHHHHHHAGPQGGFGATGGASAGLISRVANALANTSTLRTVLRTGVSQQ
IASSVVQRAAQSLASTLGVDGNNLARFAVQAVSRLPAGSDTSAYAQAFSSALFNAGVL
NASNIDTLGSRVLSALLNGVSSAAQGLGINVDSGSVQSDISSSSSFLSTSSSSASYSQASA
SSTSGAGYTGPSGPSTGPSGYPGPLGGGAPFGQSGFGGSAGPQGGFGATGGASAGLISR
VANALANTSTLRTVLRTGVSQQIASSVVQRAAQSLASTLGVDGNNLARFAVQAVSRLP
AGSDTSAYAQAFSSALFNAGVLNASNIDTLGSRVLSALLNGVSSAAQGLGINVDSGSV
QSDISSSSSFLSTSSSSASYSQASASSTSGAGYTGPSGPSTGPSGYPGPLGGGAPFGQSGF
GQRGPRSQGPGSGGQQGPGGQGPYGPSAAAAAAAAGPGYGPGAGQQGPGSQAPVAS
AAASRLSSPQASSRVSSAVSTLVSSGPTNPASLSNAISSVVSQVSASNPGLSGCDVLVQA
LLEIVSALVHILGSSSIGQINYAASSQYAQLVGQSLTQALGGGNERALTL

Figure 2.1: Amino Acid Sequence of N_BSilk. The NGF binding motif added to the N and C-termini of the recombinant aciniform protein is highlighted in yellow. The H_6 tag follows the N-terminal binding motif, shown in orange. The 2, 200 amino acid repetitive W units from A. trifasciata are shown in blue, with the first residue of the second repeat unit (S) highlighted in red. Lastly the C-terminal domain is shown in green.

The plasmid vectors and recombinant genes used to produce this protein were kindly provided by Dr. Lingling Xu and generated using methods outlined in Xu *et al.,* 2012a, then modified to include the NGF-β binding motif using methods outlined by Xu *et al.,* 2017. I assisted with constructing the expression plasmid, $pEN_BHW_2C_{ma2}N_B$. To do this, I isolated the HW_2C_{ma2} DNA fragment (1734 bp) from the cloning vector, $pDHW_2C_{ma2}$, by digesting at *Bsa1* and *BfuA*1 restriction endonuclease sites. I then ligated this fragment into the expression vector at the *Nde1* cut site to produce the final

expression plasmid. To confirm cloning was successful the expression plasmid was sequenced by Sanger Sequencing (Genewiz, NJ).

2.2.1 Protein Expression and Purification

The N_BSilk protein was expressed in Rosetta (D) *E. coli* cells using standard protocols. Briefly, a single colony of cells grown on ampicillin resistant lysogeny broth (LB) agar plates overnight at 37 ºC was used to inoculate a starter culture in 50 mL LB medium containing 50 µg/mL ampicillin. The starter culture was left to grow overnight at 37 °C while shaking. Starter culture (5 mL) was added to 3 L total of LB medium and left to grow at 37 °C for 4 h with shaking. Protein expression was then induced at 37 °C with 0.8 mM isopropyl β-D-1-thiogalactopyranoside (IPTG) for 3 h. Following induction, cells were collected by centrifuging at 4550 x g for 40 min at 10 °C. The cell pellet was resuspended in native lysis buffer (50 mM NaH_2PO_4, pH 7.79) and protein was harvested using French pressure cell lysis (886 psi; American Instrument Company). The cell lysate was centrifuged at 12 000 x g for 40 min at 4°C. As the N_BSilk construct was predominantly insoluble, the supernatant was discarded and the pellet resuspended in guanidine hydrochloride (GuHCl) lysis buffer (6 M GuHCl, 100 mM NaH_2PO_4, 10 mM TRIS-Cl, pH 8.0) before column purification. The resuspension was loaded onto immobilized Ni-NTA Sepharose resin (Qiagen, Germany), washed using 3 M GuHCl, 100 mM NaH_2PO_4, 10 mM TRIS-Cl, 10 mM imidazole, pH 8.0, and eluted from the column using 3 M GuHCl, 100 mM NaH_2PO_4, 10 mM TRIS-Cl, 250 mM imidazole, pH 8.0. The eluted purified protein was dialyzed against distilled water in cellulose tubing (14 kDa tubing, 28.7 mm wet diameter, 6.45 mL/cm volume; BioDesign) to remove salts.

The water was changed every 2 h, four times, then left overnight. The dialyzed sample was lyophilized and stored at -20 ºC for future use.

Cell lysate and protein samples from various stages of the purification process were resolved by sodium dodecyl sulfate-polyacrylamide gel electrophoresis (SDS-PAGE) in 10% acrylamide gels at 200 V for 45 min at room temperature to determine the fractions in which the recombinant N_BSilk construct were present. Gels were visualized using Coomassie Brilliant Blue R-250 staining. An unstained protein molecular weight marker with seven bands ranging from 14.4 kDa to 116 kDa (Thermo Fisher, 26610) was used to compare electrophoretic mobility of proteins present in each sample and identify N_BSilk based on its expected molecular weight (55 kDa).

2.2.2: N_BSilk Film Casting

Lyophilized N_BSilk was resuspended at concentrations ranging from 1.25% to 5% (w/v) in a variety of solvent mixtures based upon those demonstrated to be suitable for recombinant aciniform silk wet-spinning (Weatherbee-Martin *et al.,* 2016; Xu *et al.,* 2019). These included variations on the previously evaluated spinning dopes: 1,1,1,3,3,3-hexafluoro-2-propanol (HFIP) and H_2O (7:3 or 8:2, v:v) and trifluoroacetic acid (TFA), trifluoroethanol (TFE) and H_2O (8:1:1 v:v:v), as well as an alternative fluorinated alcohol mixture TFE:H_2O (7:3), to determine the optimal solvent for film-casting. N_BSilk was allowed to incubate in the solvent for 30 min at room temperature with vortexing every 10 min to facilitate homogeneity. Samples were then centrifuged for 30 min at 20 000 x g and 10 ºC. The protein suspension was pipetted onto a glass slide or into a 96-well plate (VWR: 734-278) in 2.5 µL aliquots to cast films. The films were incubated in a fume hood to allow the solvent to evaporate. The films were then cured with three 70% ethanol

washes for 10 min each, followed by solvent removal by pipetting and allowing any residual solvent to evaporate in a fume hood. A schematic of the film casting process is shown below in Figure 2.2. Films were analyzed optically using bright field microscopy at 10x with a Nikon Eclipse Ti Epifluorescence Microscope.

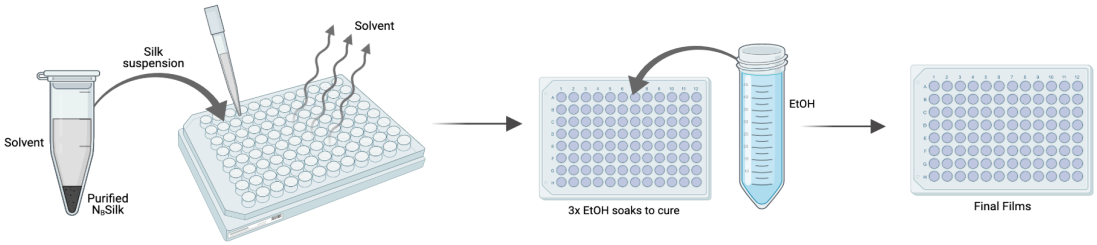

Figure 2.2: Silk Film-Casting Schematic. The flow chart for creating N_BSilk films shows how the lyophilized protein is first solubilized and the suspension is aliquoted to the wells of a 96-well plate. Once the solvent dries and leaves behind the protein, ethanol is added as a means of curing and sterilizing the silk films.

2.2.3: Silk Film Characterization with FTIR

All data were collected with a Thermo Scientific Nicolet iN10/iZ10 FTIR microscope used in reflectance mode. Sample N_BSilk films (2.5% w/v) were cast and cured as described in section 2.2.2, directly on gold plated slides (Thermo Scientific: NC9297958). The gold slide was also used to collect a background measurement. All measurements were carried out using a liquid nitrogen cooled detector, spectral range of 800-4000 cm^{-1}, 1.93 cm^{-1} resolution, and an aperture of 100 x100 μm with averaging of 64 scans at room temperature. The data were collected and processed using Thermo Scientific Omnic software. The Amide 1 region (1600 – 1700 cm^{-1}) was analyzed for peak intensity at various spectral ranges to probe for protein secondary structure characteristics, according to values from the literature (Delfino *et al.,* 2013; Yan *et al.,* 2017), which are listed for reference below in Table 2.1.

Table 2.1: Characteristic Protein Secondary Structure Peak Positions of the Amide 1 Region.[a]

Secondary Structure	Range (cm-1)	Average (cm-1)
α-helix	1648-1657	1654
antiparallel β-sheet	1612-1641	1625
	1670-1694	1682
parallel β-sheet	1626-1640	1633
β-turn	1660-1684	1673
random coil	1640-1650	1645

[a]The data are reproduced from Yan *et al.,* (2017).

2.2.4: Emission Spectroscopy Evaluation of NGF and Silk Interaction

Fluorescence spectroscopy was conducted using a PTI QuantaMaster 4 spectrofluorometer. Emission measurements were performed in triplicate, with each replicate being the average of 3 scans. To examine if the intrinsic tryptophan fluorescence of NGF is altered in the presence of N_BSilk, emission was measured over 305 to 500 nm (slit width: 5 nm) with an excitation at 295 nm (slit width: 5 nm), a step size and interval of 1 nm and an averaging time of 1 s. All measurements were performed at room temperature. NGF (human NGF-β, Shenandoah Biotechnology: P01138) and N_BSilk samples were prepared in 50 mM potassium phosphate buffer (pH 7.5) and diluted to a final concentration 5 μM in the cuvette. Samples of both the phosphate buffer and 5 μM N_BSilk were used as negative controls, as no tryptophan residues are present in the silk protein. Spectra were plotted as the mean intensity in counts+/- standard deviation.

2.2.5: ELISA Quantification of NGF-binding and Release

A modified ELISA method was used to analyze the binding affinity of N_BSilk for human NGF-β (NGF). N_BSilk films (2.5% w/v) were generated using the methods described in section 2.2.2. After the films were cured and dried, human NGF-β (Shenandoah Biotechnology: P01138) was serially diluted in phosphate buffered saline

(PBS:VWR: CAAAJ61196-AP) from the 0.1 mg/mL stock, 100 µL aliquots were added onto the films in concentrations of 5, 10, 50, 100, 150 and 200 ng/mL, and measured as a single experiment with 4 internal replicates. Preloaded NGF was allowed to incubate on the films overnight at 4 ºC to bind. The following day, the solution was removed and films were washed with 0.1% Tween 20 in PBS (PBST). Films were then blocked with 1 % BSA in PBST for 2 h at room temperature while shaking. After the blocking solution was removed, films were incubated overnight at 4 ºC with rabbit anti-NGF-β primary antibody, diluted 1:1000 in 1% BSA in PBST (EMD Millipore, AB1526). Films were then washed three times for 10 min with PBST and incubated with the anti-rabbit IgG HRP-conjugated secondary antibody, diluted 1:1000 in 1% BSA in PBST (R&D Systems, HAF008) for 1 h at room temperature while shaking. Films with no addition of NGF were also probed with antibodies as negative controls to preclude the possibility of nonspecific binding. As a positive control, and to ensure affinity of the antibody for NGF was concentration dependent, an ELISA standard curve was generated with the same concentrations of NGF aliquoted directly to the 96-well plate with no N_BSilk films. After incubation with the secondary antibody, all wells were washed again three times for 10 min with PBST. Finally, SuperSignal™ ELISA Pico Chemiluminescent Substrate (Thermo Scientific) was added to each well and incubated for 2 min before the luminescence signal was detected using a Filtermax F5 Microplate Reader. Data were plotted in GraphPad Prism 9 as the mean of relative luminescence units (R.L.U) +/- the SEM for each concentration of NGF. The relationship between R.L.U as a function of NGF concentration was fit based on the standard curve and the residuals were plotted to further analyse the relationship between NGF and the primary antibody.

A similar experiment was conducted to determine if the binding of NGF was dependent on the concentration of N_BSilk in the film. The binding ELISA method described above was followed again but using 1.25, 2.5 and 5% (w/v) films and applying NGF at 5, 10 and 50 ng/mL in 100 µL aliquots. Films with no addition of NGF were once again probed with antibodies as negative controls to preclude the possibility of nonspecific binding. All antibodies and detection methods remained the same as previously described. Data were plotted in GraphPad Prism 9 as the mean R.L.U +/- SEM for each condition. Binding affinity between conditions was compared statistically using a two-way ANOVA and Tukey's multiple comparisons test.

The release of NGF from N_BSilk films was also characterized using ELISA-based methods. N_BSilk films (2.5% w/v) were cast in a 96-well plate, preloaded with 200 ng/mL NGF and allowed to incubate overnight at 4 ºC, as with the previous experiments. Films treated with PBS only served as the negative control. Following incubation, the remaining solution was removed and each film was washed with PBST. The films were then incubated in PBS at room

temperature to probe for the release of bound NGF in the preloaded condition compared to the negative control. The PBS supernatant from each film was collected after 72 h of soaking and aliquoted into new wells containing no N_BSilk. The supernatant was left in the new wells overnight at 4 ºC to allow any NGF to bind to the plate. The wells were then probed for NGF using the same antibody and chemiluminescent detection procedure as previously described. Data were plotted in GraphPad Prism 9 as the mean R.L.U +/- SEM and compared statistically using an unpaired t-test.

2.3: Results and Discussion

2.3.1: Protein Expression and Purification

N_BSilk was first tested for its ability to express in *E.coli* cells before proceeding to large scale protein production. Similar protocols to those described in section 2.2.1 were used on a smaller scale (1 mL total culture medium) for test expressions. Following IPTG induction, cells were collected by centrifugation and then boiled in denaturing SDS-PAGE loading buffer for 15 min to induce cell lysis. The total cell lysates were resolved by SDS-PAGE, shown in Figure 2.3, and compared to a lysate from an uninduced sample (U). The enhanced band between 45 and 66 kDa, highlighted in the red box, indicates the expected electrophoretic mobility of N_BSilk and demonstrates successful overexpression of the protein through IPTG induction.

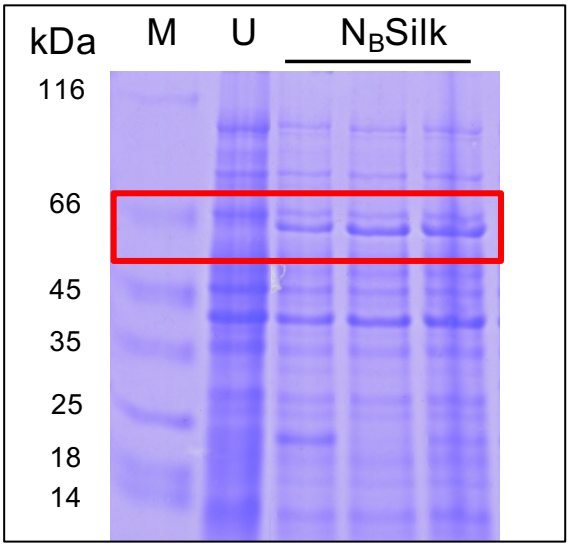

Figure 2.3: N_BSilk Expression is Successful in Rosetta Cells Following IPTG Induction. Following IPTG induction, cells were boiled to release their contents and the lysates were resolved by SDS-PAGE (Coomassie Blue stained) to check for the expression of N_BSilk. The induced N_BSilk samples (analyzed in triplicate) were compared to a cell lysate from uninduced cells (U). The red box highlights the expected electrophoretic mobility of N_BSilk at 55 kDa and shows the additional protein band present from overexpression. The above gel image was cropped to place the induced N_BSilk samples directly next to the uninduced sample for easier visual comparison of the induction results. The uncropped, full gel image is shown in Figure A1.

Following expression in Rosetta *E. coli* cells, purification of the recombinant N_BSilk had to be optimized. Previous recombinant aciniform constructs in our lab have used an N-terminal hexahistidine (H_6) tag and a SUMO tag to modify protein solubility, increase stability, facilitate purification, and increase protein yield (Xu *et al.,* 2019). The H_6 tag of N_BSilk is likely to be less available due to the fusion of the NGF-binding motif on the N-terminal of the construct, resulting in an internal H_6 tag. Furthermore, N_BSilk needed to be solubilized in order to load the protein onto a nickel-affinity column to be able to use the H_6 tag for purification purposes. As spider silk is typically highly insoluble due to its innate purpose of withstanding the natural elements, and this recombinant construct did not contain a SUMO tag, previously used protocols were altered to make this process more feasible. SUMO tags are often used to increase recombinant protein solubility; however, the exact mechanisms remain unclear. Main hypotheses for how SUMO tags facilitate solubility include: forming micelle-like structures, acting as chaperones to prevent protein aggregation, or by inhibiting protein aggregation through electrostatic interactions (Costa *et al.,* 2014).

Briefly, the recombinant protein was harvested from the collected *E. coli* cells by lysis from the insoluble, which was important for determining where the N_BSilk construct would be present and influence the purification protocol. Important steps of the purification process were resolved by SDS-PAGE, as shown in Figure 2.4. The expected electrophoretic mobility of N_BSilk was calculated to be ~55 kDa, which is highlighted by the red box in Figure 2.4. As expected, the majority of the silk protein was insoluble and present in the pellet of the cell lysate, (shown in Figure 2.4, lane "P"). Following the observation that this construct was insoluble after cell lysis, the pellet portion was re-

solubilized using a strong chaotropic agent, 6 M GuHCl, in the lysis buffer prior to being loaded onto the affinity column to isolate N_BSilk from any contaminants. Another protein appeared to be present in the insoluble portion at ~37 kDa, observed by SDS-PAGE. By solubilizing the pellet sample in GuHCl buffer and passing the solution through an affinity column, separation of N_BSilk was achieved. This also indicates that the other insoluble protein observed was likely a contaminant, and not truncations of N_BSilk, as none bound to the column. This is shown by the electrophoresis of samples that were eluted off the column following wash steps, in lanes E1 and E2 of Figure 2.4. Only one band at 55 kDa was resolved in these lanes, indicating N_BSilk was successfully isolated, providing a pure protein sample. Expression levels of N_BSilk were ~25 mg/L of culture media, which is comparable to previous aciniform silk expression studies, including HW_2C_{ma2} (Xu *et al.,* 2012a; Xu *et al.,* 2017).

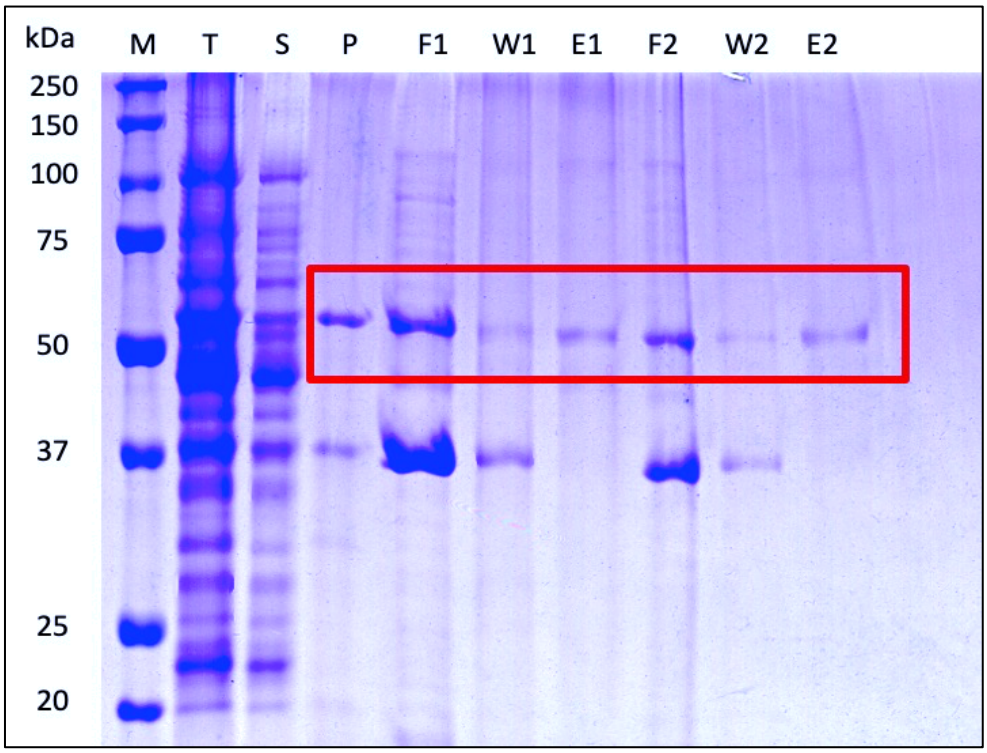

Figure 2.4: N_BSilk Can be Expressed in E. coli and Purified with Affinity Chromatography. The key stages of protein purification were resolved by SDS-PAGE gel (Coomassie Blue stained). First the cells are lysed to release their contents, shown in lanes T (total cell lysate), S (soluble portion from lysate) and P (pellet from lysate). N_BSilk is in the pellet, which is next solubilized in 6 M guanidine hydrochloride and purified using nickel affinity chromatography. F is the initial flow through from the column, followed by a wash of the column to remove any contaminants (W1) and the elution of the protein off the column (E1). As some protein was still present in the initial flow through (F1), this was loaded onto the column again and the process was repeated, shown by lanes F2, W2 and E2. The red box highlights the expected electrophoretic mobility of N_BSilk at 55 kDa.

These results indicate that the presence of an internal H_6 tag did not limit the ability of the recombinant protein to be purified via affinity chromatography. This allows more flexibility when designing future recombinant silk constructs with other N or C-terminal fusions. Furthermore, developing a method to solubilize recombinant aciniform constructs for affinity chromatography without the need of a SUMO tag, reduces the number of steps in the overall purification process without decreasing protein yield.

2.3.2: Optimization of Solvent for Silk Film Casting

Fluorinated organic solvents and acids mixed with water have been previously shown by our group to solubilize recombinant spider silks (Weatherbee-Martin *et al.,* 2016; Xu *et al.,* 2019; Simmons *et al.,* 2019). The ability to solubilize silk proteins is critical for producing materials such as films and fibres. As each recombinant construct has structural differences, identifying a solvent that was appropriate specifically for N_BSilk film-casting was essential.

Some of the solvents that were previously used for aciniform silk fibre wet-spinning dopes in our lab were tested for their ability to solubilize N_BSilk (Weatherbee-Martin, 2016; Xu *et al.,* 2019). As this work focused on silk films as opposed to fibres, the desired concentration of protein in suspension could be much lower (2.5-5%) than for fibre spinning (~5-15%), which made solubilization more feasible. Evolutionary pressure has allowed spider silks to become extremely robust macromolecules that are able to withstand the natural elements, such as wind and rain. Because of this, solubilization has been one of the limiting factors to studying both natural and recombinant spidroins (Spieß *et al.,* 2010). Solubilization of silk protein is necessary for the production of films and fibres, especially to produce fibres that are representative of those found in nature. This solubilization step mimics what occurs in the glands of spiders where the spinning dope is created before being extruded through the duct to produce the fibre. One characteristic of the gland is a pH gradient that becomes more acidic as the suspension moves through the spinning duct. It is thought that this pH change helps promote molecule assembly and plays a role in fibre formation (Heidebrecht and Schiebel, 2013). As such, acidic solvents achieve solubilization of recombinant aciniform silk constructs,

especially in combination with fluorinated organic solvents to further disrupt the hydration shell of the protein (Spiess *et al.,* 2011; Xu *et al.,* 2019;Young *et al.,* 2012).

These types of solvents were tested for their ability to solubilize N_BSilk at concentrations of both 2.5 and 5% (w/v). The qualitative outcomes for the various solvents can be seen in Table 2.2, where it is noted that most of the fluorinated alcohol:water mixtures (HFIP and TFE) resulted in visible precipitate, indicating that they were not suitable solvents for this construct. The suspensions in HFIP were still able to be cast into films, shown in Figure 2.5 C and D; however, protein aggregation and even phase separation observed with these solvents created films with uneven topologies, which are not suitable for the proposed application.

Table 2.2: Solvent Testing and Outcomes for N_BSilk Film-Casting Optimization. The potential to suspend lyophilized protein was tested in solvent mixtures suitable for fiber wet-spinning including: TFA:TFE:H_2O (8:1:1), TFE:H_2O (7:3) and HFIP:H_2O (7:3 or 8:2). The concentration of protein in the film was also varied to optimize the film casting protocol for N_BSilk.

Solvent	% Protein (w/v)	Dissolved? (Yes/No/Partially) and Observations
TFA:TFE:H_2O (8:1:1)	2.5	Yes
TFA:TFE:H_2O (8:1:1)	5	Partially
TFE: H_2O (7:3)	2.5	No, visible precipitate
TFE: H_2O (7:3)	5	No, gel-like consistency
HFIP: H_2O (8:2)	2.5	Partially, phase separation
HFIP: H_2O (7:3)	2.5	No, phase separation
HFIP: H_2O (7:3)	5	No, visible precipitate
HFIP: H_2O (8:2)	5	No, visible precipitate

The only solvent able to partially solubilize a 5% sample was TFA:TFE:H_2O, which indicated the importance of strong acidity in the solvent. In fact, the 5% sample in TFE:H_2O could not even be cast into a film due to the gel-like nature of the solution, which is why there is no representative image for films cast from this solvent in Figure 2.5. The 5% sample in TFA:TFE:H_2O still contained some protein aggregates, which can

be observed throughout the film in Figure 2.5 B. The lower concentration of protein (2.5% w/v) in the same ratio of TFA:TFE:H_2O was determined to be the best suspension for film-casting found from these trials. The 2.5% film cast from TFA:TFE:H_2O, shown in Figure 2.5 A, showed a much smoother and even topology observed through optical microscopy. A more detailed analysis of topology through atomic force microscopy would be beneficial for future work. In the case of biomaterials applications for cellular growth, a smooth film topology isn't necessarily critical; however, a uniform topology is. Many studies have indicated that surface topological features such as microgrooves, nanopatterns and even curvature can improve and guide the growth of neurons (cheng *et al.,* 2014; Smeal *et al.,* 2005; Tsuruma *et al.,* 2006). Beginning with a more uniform protein film, such as the 2.5% film in Figure 2.5 A, allows for more control during both material and cell culture experiments. A uniform film also has the potential for the controlled addition of specific and rationally-designed topological features, which could be of interest for future work.

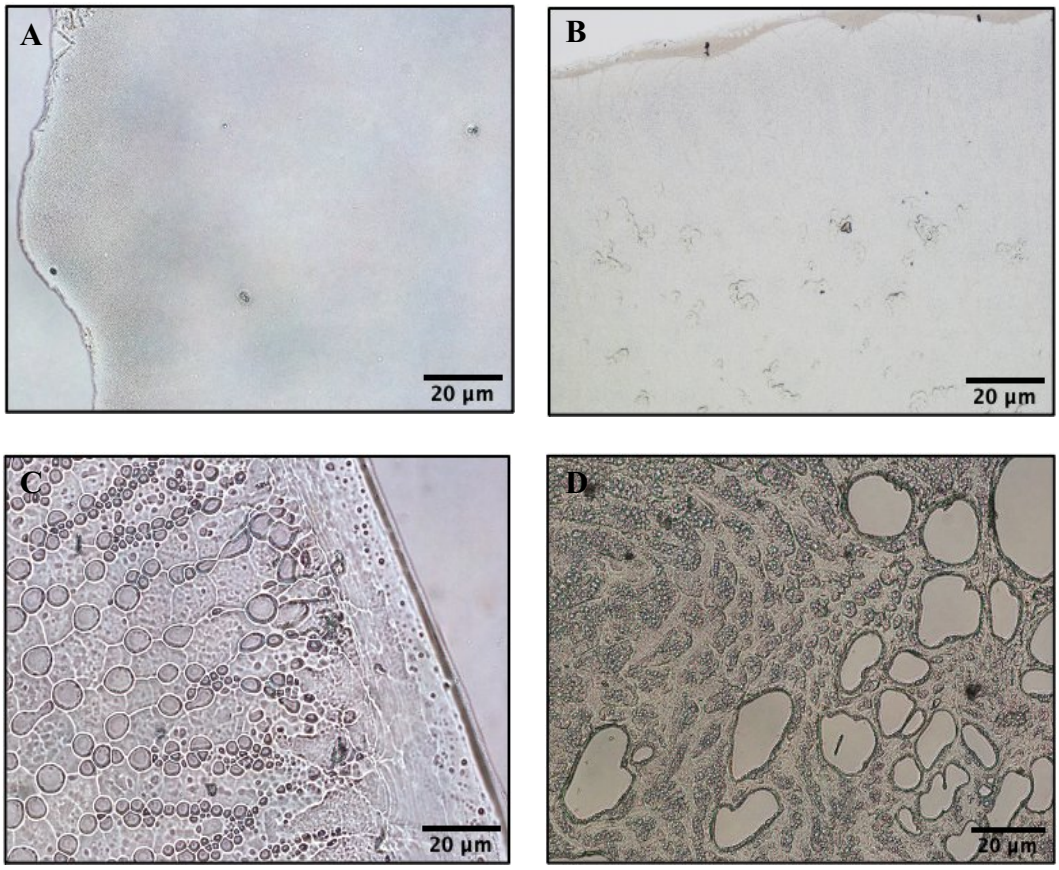

Figure 2.5: N_BSilk Suspended in TFA:TFE:H_2O Solvent Forms Optimal Films. Protein/solvent mixtures were cast onto glass slides and cured in ethanol to generate silk films, then imaged using optical microscopy. A and B show films made from 2.5% and 5% (w/v) N_BSilk suspended in TFA:TFE:H_2O, respectively. C and D show films made from 2.5% (w/v) $N_B$silk suspended in HFIP:H_2O (8:2, 7:3, respectively).

2.3.3: Film Characterization

Following the identification of appropriate film-casting conditions, I was interested to characterize the protein structural characteristics present in this form of N_BSilk. Furthermore, when the films are cast onto a large substrate such as a glass slide, one can identify the protein film optically by finding the edge and comparing the glass slide background to the film itself, observed in Figure 2.5 A, B and C. In addition to demonstrating this optically, and to further prove that the protein was in fact present in films, secondary structure characteristics were probed using FTIR microscopy.

Figure 2.6 shows a representative IR spectrum of a 2.5% (w/v) N_BSilk film cast onto a gold-coated slide. Characteristic bands indicative of protein structure are observed throughout the spectrum, including those in the amide I (~1600-1700 cm^{-1}) and amide II (~1500-1600 cm^{-1}) regions. The amide I region typically provides a higher intensity signal and is, therefore, most frequently used to gather information on protein secondary structure (Delfino *et al.,* 2013). The upper right hand panel of Figure 2.6 is the same spectrum, but zoomed in to show the amide I region in greater detail. This broad band is the convolution of several component IR absorption peaks that comprise the entire area and represent contributions from individual protein secondary structure elements such as β-structures, α-helices or disordered regions. This region in N_BSilk suggests two intense component peaks at ~1650 cm^{-1} and ~1620 cm^{-1}. Based on the literature values of protein secondary structure characteristics identified using FTIR spectroscopy, peaks at these particular wavenumbers are suggestive of α-helices and β-sheet structures (likely anti-parallel sheets), respectively (Delfino *et al.,* 2013; Yan *et al.,* 2017).

Previous structural studies on silk films have focused on dragline silk (ADF4 of *A. diadematus*) and found similar results using FTIR spectroscopy. Spieß and colleagues (2010) cast ADF4 films from HFIP suspensions and observed high α-helical content; however, following treatment with methanol, the films shifted to a more β-sheet rich structure. Aliphatic alcohols have previously been demonstrated to promote of this structural rearrangement in silks, a property that is often exploited during the fibre-spinning process. As N_BSilk films are soaked in ethanol as part of the curing and sterilization protocol, this similar structural phenomenon was to be expected and aligns with the results of the shown FTIR spectrum. In order to fully tease apart the total content

of unique structures which comprise the overall amide I peak, accurate deconvolution of the spectrum is a necessary next step.

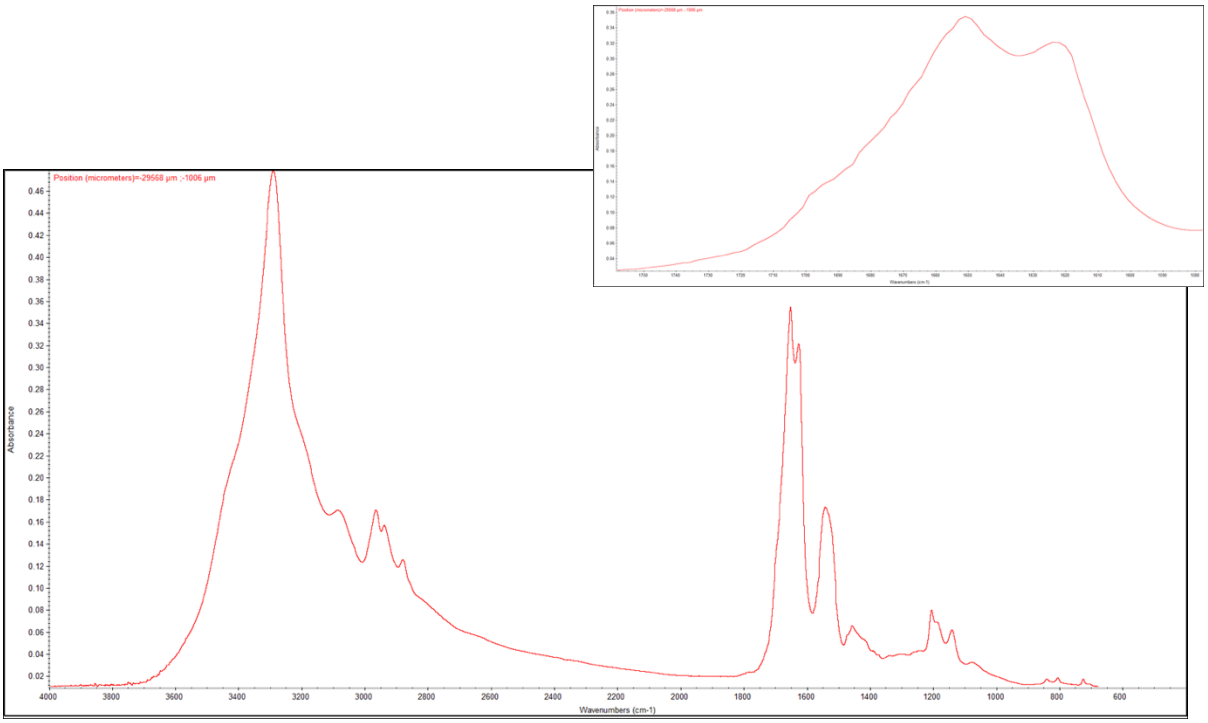

Figure 2.6: FTIR Spectroscopy of N_BSilk Films Indicates the Prescence of Protein Structure. Representative FTIR spectrum of 2.5% (w/v) N_BSilk films cast using the TFA:TFE:H_2O (8:1:1) solvent onto gold plated slides and cured in 70% ethanol. Spectra were collected in reflectance mode using the gold slide as a background measurement. The data were collected and processed using Thermo Scientific Omnic software. The upper righthand panel shows a close up image of the Amide I region of the spectrum (1600 – 1700 cm^{-1}).

Following initial protein production and characterization, the next main goal was to identify whether the NGF binding motifs that were fused to either terminus of the protein were functional. Since the 3D structure of the recombinant protein has not been studied, the accessibility and availability of these motifs remained unknown. Although N_BSilk was mainly studied in film form during this project, to directly probe the interaction between N_BSilk and NGF without the need for additional protein modification or labelling, solution-state experiments were employed using fluorescence spectroscopy. This experiment exploited intrinsic tryptophan residues present in NGF. Tryptophan is a

sensitive and frequently employed fluorophore in proteins. Since NGF contains Trp residues while N_BSilk does not, I was able to compare the fluorescence before and after exposure to N_BSilk, and look for any shifts in the emission spectrum that might indicate a change in NGF conformation and suggest interaction between the molecules. A structural diagram of the biologically active form of human NGF-β, which is a homodimer in complex with the high affinity receptor, TrkA, is shown in Figure 2.7. The NGF molecules are shown at the centre of the complex in green and orange with their Trp residues shown as ball and stick models for reference.

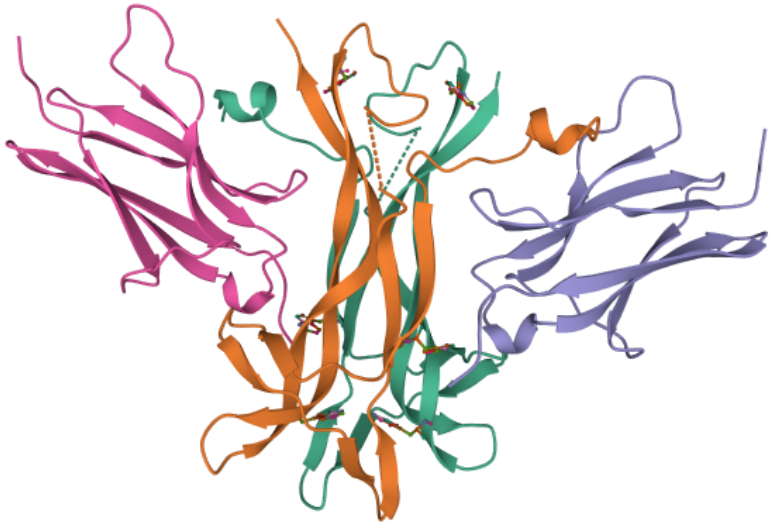

Figure 2.7: Biologically Active Structure of NGF in Complex with Domain 5 of the TrkA Receptor. Schematic of NGF homodimer (green and orange) in complex with TrkA receptors (pink and purple). Tryptophan residues of NGF molecules are shown as ball and stick models. Crystal structure determined using X-ray diffraction. Reproduced from Weismann et al., (1999), with permission from Springer Nature.

The sample containing only NGF exhibited a strong emission peak at ~340 nm, as expected for Trp in solvent-exposed conditions, shown in Figure 2.8. When combined in solution with N_BSilk the wavelength of the emission maximum did not shift; however,

the signal intensity decreased. This could indicate that the silk is interacting with NGF, as the concentration of NGF in solution was the same for both conditions. Three Trp residues are present in NGF so depending on the interaction between NGF and the binding motif of N_BSilk, only some of these residues may become perturbed resulting in a decreased emission intensity. The observed change in intensity corresponds to previous NGF structural studies in the literature, such as with Zhao *et al.,* (2004) who showed a shift in the fluorescence intensity, but not the wavelength of NGF in response to the addition of Zn(II).

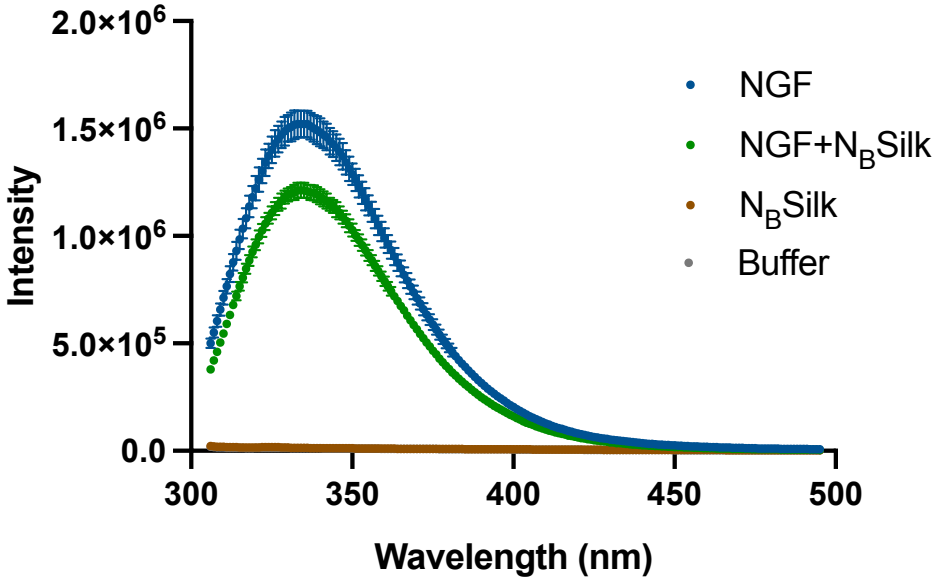

Figure 2.8: Fluorescence Spectroscopy Reveals Interaction Between N_BSilk and NGF. Intrinsic tryptophan fluorescence of 5 µM human NGF-β (λex = 295 nm) in 50 mM KPO_4 buffer (pH 7.5) or in solution with N_BSilk. A sample of buffer alone was used as a background measurement and a sample of 5 µM N_BSilk in buffer was used as a negative control. Fluorescence is shown as mean intensity counts +/- the SEM.

Although this experiment may suggest an interaction between NGF and N_BSilk in solution, more work was needed to prove the ability of the silk films to bind NGF, since the main focus of this project pertains to silk in film form. Nonetheless, due to the

unknown binding mechanism of the motif fused to the recombinant silk to create this construct, future fluorescence spectroscopy experiments, such an anisotropy measurements, may still provide insight into the nature of this interaction.

With fluorescence spectroscopy suggesting that the molecules in solution are interacting, I next tested if NGF would bind to N_BSilk films. A method had to be designed and optimized in order to quantitatively detect NGF on the silk films. An immunoassay approach was taken and the standard sandwich ELISA protocol was adjusted to incorporate N_BSilk (Abcam, 2018). A schematic of this methodology is shown in Figure 2.9 A, where N_BSilk films are first cast into a 96-well plate as previously described in section 2.2.2. The films therefore acted similarly to a capture antibody, where NGF was aliquoted onto N_BSilk films at varying concentration and allowed to bind, before washing, blocking and detection steps of the procedure.

The binding ELISA detection method first had to be optimized, so a similar experiment was conducted without silk present to serve as a positive control. Specifically, NGF was aliquoted in a series of increasing concentrations directly into 96-well plates prepared without an N_BSilk film coating. This allowed me to test for the capability of the antibody to bind to NGF in a concentration-dependent manner. In this control experiment, chemiluminescent detection signals were only observed in the presence of NGF with limited non-specific binding (Figure A2).

Following validation of this technique, the binding ELISA was conducted with N_BSilk films (Figure 2.9 B). Under these assay conditions, NGF appears to bind to the films in a concentration dependent manner, albeit in a nonlinear manner, with increasing chemiluminescent signal detected for films that were incubated with higher

concentrations of NGF. As we do not know the 3D structure of this recombinant aciniform construct, it was previously unknown if the binding domains and how many, would be readily available at the surface of the film. This assay, therefore, provides confidence that the binding sequence fused to N_BSilk is still accessible while the protein is in film form.

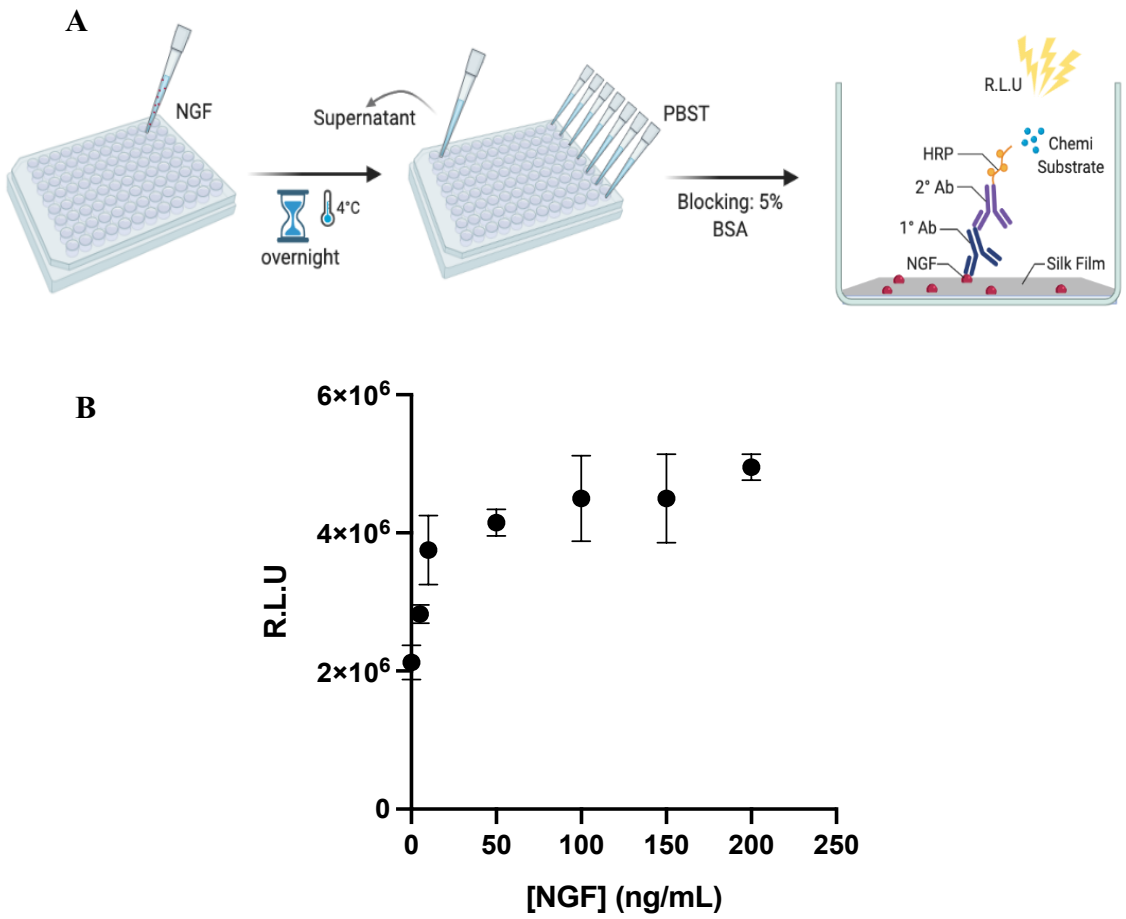

Figure 2.9: A) Development of ELISA Method for Analysis of NGF-Binding Capabilities of N_BSilk. A) shows a schematic representation of how a standard sandwich ELISA protocol was altered to assess the binding affinity of N_BSilk for NGF. Refer to figure 2.2 for the initial steps of film-casting into the 96-well plate. **B) NGF Binds to N_BSilk in a Concentration Dependent Manner.** The ability for N_BSilk films to sequester and release NGF was tested with the ELISA-based method shown in figure 2.6a. Films were loaded with NGF of concentrations ranging from 0 ng/mL to 200 ng/mL and allowed to bind overnight. NGF was detected using a primary antibody bound to a horse radish peroxidase- conjugated secondary antibody and chemiluminescent substrate to measure relative luminescence units (R.L.U). Film luminescence was measured in triplicate for each condition, from a single experiment and plotted as the mean +/- SEM.

To determine if the concentration of silk protein employed for film casting affected the affinity for NGF, the binding ELISA was repeated using 1.25, 2.5 and 5% (w/v) N_BSilk films (Figure 2.10). The same experiment was conducted using low to mid-range concentrations of NGF (0-50 ng/mL), as these conditions showed less variability

and a greater concentration-dependent difference in luminescence than the higher concentrations in the initial binding ELISA from Figure 2.9 B. The 2.5% films did not differ in their affinity for NGF from the 5% films; however, films cast at both of these concentrations differed significantly from the 1.25% film. Specifically, the binding of NGF is observed to be dependent on the concentration of N_BSilk, but only when comparing the two film conditions cast using lower concentrations of protein (1.25% vs. 2.5% w/v). Recalling the optical microscopy data for the films in Figure 2.5, this assay provides further support for the specific choice of casting films at a concentration of 2.5% (w/v). Namely, the lower protein concentration employed in the 2.5% (w/v) conditions which allows for casting of a more uniform film relative to the 5.0% (w/v) films does not significantly attenuate the NGF binding capacity of the films.

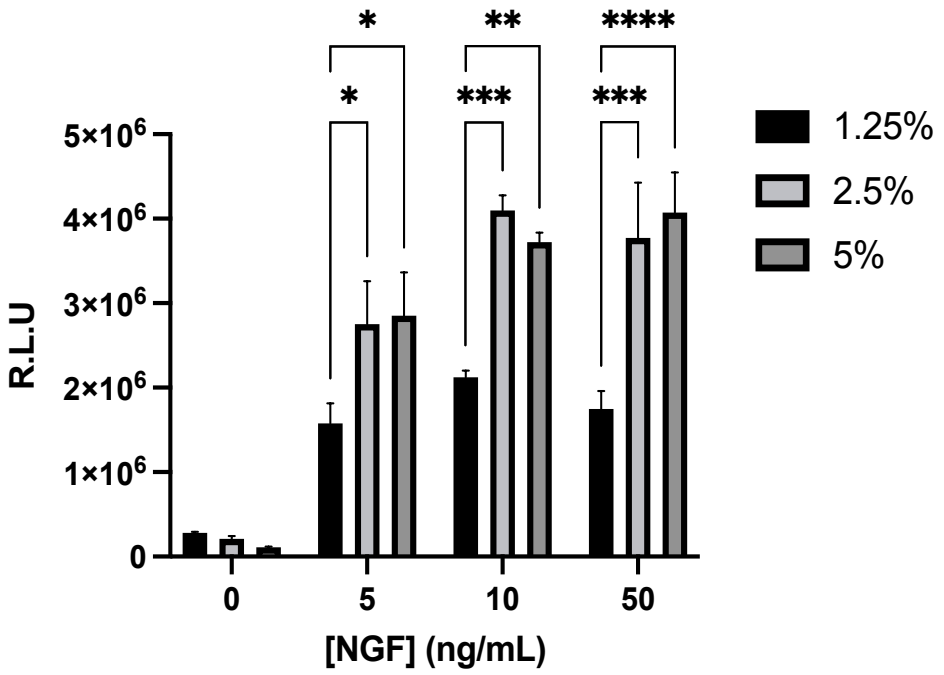

Figure 2.10: NGF Binding Is Further Dependent on the Concentration of N_BSilk. The ability for N_BSilk films to sequester and release NGF was tested with the ELISA-based method shown in figure 2.6a. Films of either 1.25, 2.5 of 5% w/v protein were loaded with NGF of concentrations ranging from 0 ng/mL to 50 ng/mL and allowed to bind overnight. NGF was detected using a primary antibody bound to a horse radish peroxidase- conjugated secondary antibody and chemiluminescent substrate to measure relative luminescence units (R.L.U). Film luminescence of each condition was measured in quadruplicate from a single experiment and plotted as the mean +/- SEM. Statistical significance was computed using a two-way ANOVA and Tukey's multiple comparisons test. * = $p<0.05$, ** = $p<0.005$, *** = $p<0.0005$, ****= $p<0.0001$.

After determining that the N_BSilk films were able to bind NGF, I was also interested to see if they would release the growth factor over time. Many biomaterials that are bound or loaded with small molecules such as growth factors exhibit a burst release once the material is in a hydrated environment. A burst release results in the loss of all loaded small molecules immediately from the material, as opposed to slowly over time. For biomaterials that are meant to exert a sustained effect, an initial burst release of

the loaded molecule is unfavorable and remains a challenge in biomaterials development (Wang *et al.,* 2017).

After allowing NGF to bind, films were soaked in PBS for defined periods of time to investigate the release of NGF. Initial work showed no detection of NGF in the first few hours to 1 day of soaking. It is possible that NGF was being released at levels below the detection limit of the ELISA; however, in order to get a better idea if any was being released at all, preloaded films were soaked for 72 h as a longer time point. If NGF release occurred in a time-dependent manner, this longer release time would provide an increase in the likelihood of detection via ELISA. After 72 h, the supernatant from preloaded N_BSilk indeed showed a significantly increased signal compared to the negative control, shown in Figure 2.11. This confirmed that NGF is being released by N_BSilk films and indicated that it may be releasing slowly over time, in concentrations below the detection limit of the ELISA.

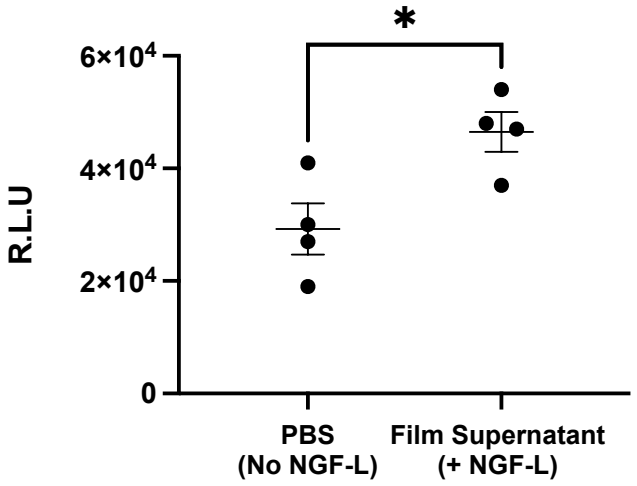

Figure 2.11: NGF Releases from N_BSilk Slowly in Detectable Concentrations After 72 h. Following loading with 200 ng/mL NGF (NGF-L), films were soaked in PBS for 72 hours and the supernatant was taken to probe for NGF released via ELISA. Films incubated with PBS only (no NGF-L) served as the negative control. Detection of NGF is measured as relative luminescence units (R.L.U) and quadruplicate samples from a single experiment were plotted as the mean +/- SEM. Statistical significance was measured using an unpaired t test. * = $P \leq 0.05$.

Little and slow release may not be appropriate for all growth factor-releasing biomaterial applications, but fortuitously this is entirely suitable for application of NGF-loaded materials for nerve regeneration. Some ligand-receptor interactions require internalization at the plasma membrane and this was initially thought to be the case with NGF and its receptor, TrkA (Watson *et al.,* 1999). It was later found that NGF bound to a substrate is sufficient to initiate signaling (MacInnis and Campenot*,* 2002). Specifically, this was shown through the phosphorylation of AKT in rat sympathetic neurons that were exposed to NGF which was covalently crosslinked to beads, rendering it immobilized. The observation of this phosphorylation suggested that TrkA could be phosphorylated at the plasma membrane and activate PI3 kinase to continue downstream signal transduction, without the necessity for internalization (MacInnis and Campenot*,* 2002). Thus, if a high concentration of NGF remains sequestered by N_BSilk, neuronal cells grown on this substrate can potentially still be stimulated by the growth factor even in the absence of substantial NGF release. This may even be advantageous by keeping the effects of the biomaterial at the site of interest and increasing accessibility of the growth factor to cells due to proximity. The bioactivity of the NGF either immobilized or released into this system by N_BSilk will be discussed in detail in Chapter 3.

2.3.4: Conclusions

In this chapter I demonstrated the feasibility of producing the recombinant aciniform construct, N_BSilk, and its ability to be cast into films for biomaterial applications. I showed the presence of protein within these silk films using FTIR spectroscopy and suggested distinct secondary structure characteristics that may be

present. In solution, an interaction between the binding motifs of N_BSilk and NGF was suggested by a shift in fluorescence intensity, indicating some of the Trp residues of NGF may have been perturbed. When cast into protein films, the NGF-binding sequence remained accessible on N_BSilk, as NGF bound in a concentration dependent manner and released slowly over time. This characterization provided the rationale to move forward with cell culture experiments to determine the bioavailability of NGF sequestered by N_BSilk films and its potential for tissue engineering applications.

Chapter 3 : N_BSilk Films Support Growth of Neuronal Cells

3.1: Overview and Experimental Objectives

In Chapter 2, the recombinant silk protein, N_BSilk, was successfully produced and cast into films for potential biomaterial applications. Materials studies with the N_BSilk films suggested it had the ability to sequester the neurotrophic factor, NGF. To test the biocompatibility of this material with cells, as well as the bioavailability of the sequestered NGF for future nerve regeneration applications, I conducted *in vitro* experiments analyzing the differentiation of PC12 cells in response to growth on N_BSilk. For materials that are developed to assist with nerve regeneration, the promotion of neurite outgrowth is a main goal. Synapse formation is a critical step in nerve regeneration and cannot occur without the proper formation of axons (Schwab and Bartholdi, 1996). In the PNS, Schwann cells upregulate the expression and secretion of NGF at the distal stump in response to axotomy, which triggers the release of cytokines and other growth factors to further promote regeneration (Frostick *et al.,* 1998). The lack of Schwann cells and their signalling capabilities, in addition to low endogenous levels of NGF in the spinal cord, are some of the main challenges when it comes to nerve regeneration in the CNS (Krenz and Weaver, 2000).

The accumulation of NGF has been observed in both the distal and proximal ends of the spinal cord in rats following traumatic injury. Furthermore, immune cells that invade the area following injury were observed to be secreting NGF localized to the axon-like structures emerging from the injury site (Murakami *et al.,* 2002). This led to the hypothesis that NGF plays a critical role in reinnervation of the spinal cord following injury. Thus, the use of exogenous NGF has been proposed and studied for both PNS and

CNS injuries. Ultimately, off-target NGF-induced axon sprouting was a major issue and led to side effects such as chronic pain and abnormal reflexes (Krenz *et al.,* 1999). These limitations only provide further motivation for the study of controlled NGF release from biomaterials; such as N_BSilk. The results of section 2.3.3 revealed that NGF was released slowly and in only small quantities from N_BSilk, with most of the NGF retained on the silk scaffold. If the bound NGF remains bioactive and available to cell surface receptors, this would help to ensure limited off-target effects *in vivo.* Additionally, biomaterials that can sequester and enhance the presentation of endogenous NGF at the site of injury, as well as NGF being secreted from inflammatory immune cells, could prevent adverse effects of NGF on off-target, surrounding cells. Thus, biomaterials such as films or fibres made from N_BSilk may be suitable to address these issues. This chapter focuses on PC12 cells as a model system to assess NGF-induced differentiation in response to N_BSilk as a growth substrate. Multiple cell culture experiments were used to investigate both optically, and at the molecular level, for the ability of N_BSilk to promote the critically important process of neurite outgrowth.

3.1.1: PC12 Cell Lines as Model Systems

PC12 cells were specifically selected for these studies due to their ability to differentiate into neuron-like progenitor cells in response to NGF signaling. The PC12 cell line was derived from rat pheochromocytoma, a typically benign tumor of the adrenal glands (Greene and Tischler, 1976). These cells are a commonly used model system for many types of signaling studies due to their ability to respond to growth factors, hormones, and most notably for the present work, neurotrophins (Perera *et al.,* 2019). There are two different variations of PC12 cells available as defined by the American

Type Culture Collection (ATCC), traditional PC12 cells (1721) and PC12 Adherent (Adh) cells (1721.1). Traditional PC12 cells grow in suspension at a slower rate, compared to their adherent counterparts. Morphologically, traditional PC12 cells are small, round shaped cells that aggregate into clusters. Few, if any, individual PC12 cells or aggregates are typically observed to adhere to tissue culture plates, thus the modification of the adherent cell line. PC12 Adh cells are fast growing and polygonal in shape. They were developed by culturing PC12 cells repeatedly on Corning's CellBIND™ flasks to induce a more adherent phenotype (Wiatrak *et al.,* 2020).

PC12 cells have long been the primary method for studying neurotrophin signaling due to difficulties in culturing primary neurons. Both PC12 cell lines express the high-affinity receptor for NGF, TrkA, which is present on the plasma membrane (Jing *et al.,* 1992). Following ligand-receptor binding, TrkA dimerization and transphosphorylation occur, resulting in several signal transduction cascades. Key signaling pathways involved in cell survival, differentiation and subsequent neurite outgrowth include the PI3-K pathway MAPK pathway (Klesse *et al.,* 1999). Downstream phosphorylation targets of these pathways include AKT and ERK1/2, respectively, making the phosphorylation of these proteins ideal molecular markers of differentiation in PC12 cells. In fact, previous studies have shown that blocking Ras/ERK signaling in PC12 cells inhibits NGF-induced differentiation completely (Szeberényi and Cooper, 1990; Kremer *et al.,* 1991). For more detail of NGF-induced signalling, see Chapter 1, Figure 1.5 and the text of section 1.3.1.

Previous work has elucidated the importance of surface coatings for the culture and differentiation of traditional PC12 cells, due to their innate preference to grow in

suspension (Wiatrak *et al.,* 2020). The surface modification of tissue culture vessels has been shown to be even more important for cellular differentiation than NGF administration. Cellular adhesion promotes microfilament reorganization which in turn allows for stable neurite extension (Fuji *et al.,* 1982). Thus, by investigating both traditional and adherent variations of PC12 cells, I aimed to determine whether N_BSilk could promote differentiation and neurite outgrowth in these cell lines to prove its potential for neuronal biomaterial applications.

3.1: Materials and Methods

3.2.1: PC12 and PC12 Adh Cell Culture

Both PC12 (ATCC 1721) and PC12 Adh (ATCC CRL 1721.1) cells were used to study the ability of N_BSilk to promote nerve growth and differentiation. Cells were grown from passage 2 (PC12) or 0 (PC12 Adh) from liquid nitrogen storage. Both cell lines were cultured in 100 mm by 22 mm treated tissue-culture dishes (VWR: CABD353003) and kept in an incubator at 37 ºC with 5% CO_2. RPMI 1640 Medium (Corning: 10040CV) supplemented with 10% heat-inactivated horse serum, 5% fetal bovine serum (FBS), and 1% antibiotic antimycotic solution (Sigma-Aldrich: A5955) was used as complete culture medium for PC12 cells. For PC12 cell differentiation medium, RPMI 1640 Medium with 1% antibiotic antimycotic was used with addition of 100 ng/mL NGF (human NGF-β, Shenandoah Biotechnology: P01138) and 1% of both serums. For PC12 Adh cells, F-12K Medium (Corning: 10025CV) supplemented with 15% heat-inactivated horse serum, 2.5% FBS, and 1% antibiotic antimycotic solution was used as complete culture medium. F-12K Medium with 1% antibiotic antimycotic was used for PC12 Adh differentiation medium, but with 100 ng/mL NGF and 1% of only horse serum.

ATCC guidelines were followed when bringing both cell lines out of liquid nitrogen storage. Briefly, cells were thawed in a 37 ºC water bath for 2 min, then aliquoted into 9 mL of the appropriate complete culture medium. Suspensions were centrifuged at 200 x g and 20 ºC, for 5 min to collect the cells. The supernatant containing residual dimethyl sulfoxide for cryoprotection was removed and replaced with fresh complete culture medium for each cell line. Cells were resuspended in their respective medium and then aliquoted to tissue-culture dishes for propagation in an incubator at 37 ºC, 5% CO_2.

Both cell lines were passaged when 70-90% confluency was achieved. Until then, medium was replaced every 2-3 days, as needed. To subculture PC12 Adh cells, media was removed and the tissue-culture dish was rinsed with PBS. The cells were then incubated in 0.05% trypsin and 0.53mM EDTA in Hank's balanced salt solution (Corning: CA45001-82) for 5 min at 37 ºC to detach cells from the dish. The trypsinization was quenched by adding 5 mL PC12 Adh complete culture medium before transferring the suspension to a centrifuge tube. To subculture PC12 cells, the cell suspension was directly transferred to a centrifuge tube. Cell suspensions of both cell lines were centrifuged at 200 x g and 20 ºC, for 5 min to collect the cells. The supernatant was discarded and cells were resuspended in 5 mL of their respective complete culture medium. Cells were counted using a Countess II Automated Cell Counter (Thermo Fisher) before being aliquoted to new tissue-culture dishes for propagation, or 96-well plates for experiments.

3.2.2: PC12 and PC12 Adh Neurite Outgrowth Assay

N_BSilk films were prepared for cell culture experiments in a 96-well tissue culture plate, as described in section 2.2.2. As a positive control substrate for PC12 cells, additional wells were coated with 0.01% collagen 1 from rat tail (Corning: C980H97), since PC12 cells can adhere and extend neurites in response to NGF when grown on collagen (Wiatrak *et al.*, 2020). The collagen (50 µL) was aliquoted into the 96-well plate and allowed to bind overnight at 4 ºC. The following day, the supernatant was removed and the wells were sterilized with 70% EtOH for 10 min, repeated 3 times. Since the PC12 Adh cell line has been modified to increase adherence to plastic surfaces, the tissue-culture plate alone was used as a positive control substrate for these cells.

In the neurite outgrowth experiment, PC12 and PC12 Adh cells were grown on either N_BSilk films, 100 ng/mL NGF-preloaded N_BSilk films, or their respective positive control. Films were preloaded with NGF as previously described in section 2.2.5. Furthermore, cells seeded on each substrate were cultured in both their base differentiation medium containing no NGF, or the differentiation medium containing NGF (100 ng/mL) to promote neurite outgrowth. A single experiment contained 4 internal replicates for each condition.

PC12 and PC12 Adh cells were grown to passage 3 using the methods described in section 3.2.1, then were seeded into their appropriately prepared 96-well plate at a density of 15,000 cells/well. Each well was topped up with the appropriate differentiation medium and cells were grown in an incubator at 37 ºC, 5% CO_2 for 1 week, with medium replaced every 2 days. Images of PC12 cells were taken every second day, while PC12 Adh cells were imaged every day. A single representative image from each well was

collected using bright field microscopy with a Nikon Eclipse Ti Epifluorescence Microscope, with cells observed using a 10X objective.

3.2.3: PC12 and PC12 Adh Neurite Analysis with NeuronJ

The representative bright field microscopy images from both cell cultures were processed in Image J before analysis of neurite outgrowth with the Image J plugin, Neuron J. Images were converted to a binary by first creating an 8-bit image, then subtracting the image background and adjusting the threshold to isolate cells as particles to be counted. The number of cells per field of view was determined for each image, which was necessary for later calculations of neurite density. For the present work, neurite density is defined as the number of total neurites in the field of view, normalized by the number of cells in the field of view, and multiplied by 100 to create a percentage of total neurites observed. To count the number of neurites, 8-bit images were analyzed in Neuron J and neurites were traced. A neurite was defined as being 2 x the length of the respective cell body. Neuron J was used to count the total number of neurites that were traced on the image and calculate the average neurite length according to the scale of the image. Data were processed in Microsoft Excel, then plotted in GraphPad Prism 9 to show both neurite density and length over the period of the cell culture experiments.

3.2.4: PC12 and PC12 Adh Cell Viability Assay

Following the neurite outgrowth assay for each cell line, the cell viability and metabolic activity was probed using a CellTiter-Glo Cell Viability Assay (Promega: G9242). Briefly, following final imaging on day 7 of cell culture the assay reagent was added to each well to lyse the cells. The appropriate differentiation medium for each cell line was added to additional wells to act as a background measurement. Lysis was

facilitated by shaking 96-well plates for 2 min. The well plate was then incubated at room temperature for 10 min, followed by luminescence reading using a Filtermax F5 Microplate Reader. The data were normalized to the cell number per field of view counted on day 7 and plotted as the mean R.L.U +/- SEM, then analyzed using GraphPad Prism 9, for each cell culture substrate condition.

3.2.5: Cell Lysis and Protein Quantification

Prior to Western blot analysis, cells were lysed to release their contents. Medium was first removed from each well before adding 200 µL cell lysis buffer (Cell Signal Technology: 98035) with the addition of a protease and phosphatase inhibitor cocktail (Sigma-Aldrich: MSSAFE). Cells were incubated in the lysis buffer for 30 min, at 4 ºC while shaking. Lysates from each condition's four internal replicates were pooled to ensure high enough concentrations of protein for immunoblot detection. The pooled samples were centrifuged for 30 min at 14 000 x g and 4 ºC. The supernatant was collected while the pellet was discarded. Protein samples were either frozen at -20 ºC for future use, or protein content was determined using a Bradford assay. To obtain a standard curve in order to determine protein concentration in the cell lysate samples, a standard curve was generated using bovine serum albumin (BSA). BSA was serially diluted from a 1 mg/mL stock to create solutions of known concentrations. Bradford reagent (250 µL, Bio-rad: 5000205) was added to a 96-well plate, followed by 10 µL of BSA standard, or cell lysate sample. Samples were mixed well with pipetting, then incubated at room temperature for 10 min to allow the color to develop. The absorbance of samples was measured at 595 nm using a Filtermax F5 Microplate Reader. All samples

were measured in triplicate. Protein content of cell lysates could then be calculated from the standard curve.

3.2.6: Western Blot Analysis of pAKT and pERK Expression

The expression of pAKT/AKT and pERK/ERK1/2 in PC12 and PC12 Adh cells cultured on N_BSilk or controls was analyzed with Western blotting. Cells were cultured on the same conditions as previously mentioned in section 3.2.2, but incubated for only 30 min at 37 ºC and 5% CO_2. The 30 min incubation period was determined to be optimal for probing the phosphorylation event of AKT after preliminary time trial experiments. Following the NGF induction period, cells were lysed and protein was quantified using methods described above in section 3.2.5. The proteins in each sample were then separated by SDS PAGE in 10% acrylamide gels. Protein (30 µg) was loaded onto the gel and resolved at 100 V for 1 h, followed by 200 V for 45 min. A protein molecular weight standard ladder (Thermo Scientific: 26623) ranging from 10 to 260 kDa was also loaded to compare to the proteins detected through immunoblotting.

Proteins were next transferred from the gel to a PVDF membrane (Amersham: 1060030) for 75 min at 100 V. After transfer, the blots were rinsed in TRIS-buffered saline, 0.1% Tween 20 (TBST), then blocked for 1.5 h using 5% BSA in TBST. Primary antibodies were diluted 1:1000 in 1% BSA in TBST. Blots were incubated with primary antibodies overnight at 4 ºC, with shaking. The primary antibodies used for this experiment were as follows: AKT rabbit antibody (Cell Signal Technology: 9272), phospho-AKT (S473) rabbit monoclonal antibody (Abcam: 81283), p44/42 MAPK (ERK1/2) rabbit antibody (Cell Signal Technology:9102), phospho-p44/42 MAPK (pERK1/2, T202, Y204) rabbit antibody (Cell Signal Technology:9101).

The following day, blots were washed for 10 min with TBST, repeated 3 times. The anti-rabbit IgG HRP-conjugated secondary antibody (R&D Systems: HAF008) was then incubated with blots at room temperature for 1 hour. Another 3 washes with TBST for 10 min each was repeated before adding ECL Western Blot Substrate (Thermo Fisher: CAPI32109) for 2 min while shaking. Blots were visualized using chemiluminescent detection with an Azure c300 imaging system. Densitometry in Image J was used to measure integrated pixel intensity to compare protein expression between samples. To do this, the phosphorylated protein data were normalized to total non-phosphorylated protein, creating a ratio that could be compared statistically across groups using an ANOVA and Tukey's multiple comparison testing in GraphPad Prism 9. The results were analyzed from 3 separate experiments containing 4 internal replicates of each condition.

3.3: Results and Discussion

3.3.1: PC12 Neurite Outgrowth Assay

Since traditional PC12 cells are more extensively studied and known to directly respond to NGF by differentiating to resemble sympathetic-like neurons, they were the cell line used for initial cell culture experiments with N_BSilk (Klesse *et al.,* 1999). To investigate the function of N_BSilk as a substrate for cell growth, and the bioavailability of NGF sequestered by N_BSilk, multiple conditions were tested, including but not limited to: N_BSilk preloaded with NGF (NGF-L), N_BSilk only exposed to NGF in the cell culture medium (NGF-M), or exposed to no NGF at all. These aforementioned N_BSilk conditions were compared to the standard method of culturing and differentiating PC12 cells, which is on collagen coated tissue culture vessels to improve cellular adhesion (Wiatrak *et al,* 2020).

Upon optical analysis of the PC12 cells on N_BSilk in the presence of NGF-M, cells displayed moderate attachment to the silk substrate over the course of one week of culture (Figure 3.1 C and D). They also displayed less cellular aggregation compared to the negative control of cells grown on collagen (Figure 3.1 A) and silk alone, both with no exposure to NGF. Aggregation and growth in solution was initially of concern for N_BSilk conditions, as traditional PC12 cells typically require collagen or other ECM-component substrates to adhere and differentiate on tissue culture vessels (Wiatrak *et al,* 2020).

When PC12 cells were grown on collagen + NGF-M, they displayed signs of differentiation, such as morphological changes to initiate neurite outgrowth, after 24 h of incubation. The density of neurites in this condition peaked at day 4 of cell culture, which

is shown as a positive control to reference in Figure 3.1 B. Contrarily, the PC12 cells grown on N_BSilk required the stimulation of either NGF-M or both NGF-L and NGF-M to initiate differentiation and subsequent neurite outgrowth. Figure 3.1 C shows the cells on N_BSilk (+ NGF-L and NGF-M) on day 4, when they first showed morphological signs of initiating neurite extension. By day 7 of cell culture (Figure 3.1 D), this same condition had extended few, but long neurites emerging from clusters of cells. This optical microscopy data provided the first evidence that N_BSilk is able to support the survival and differentiation of neuron-like cells.

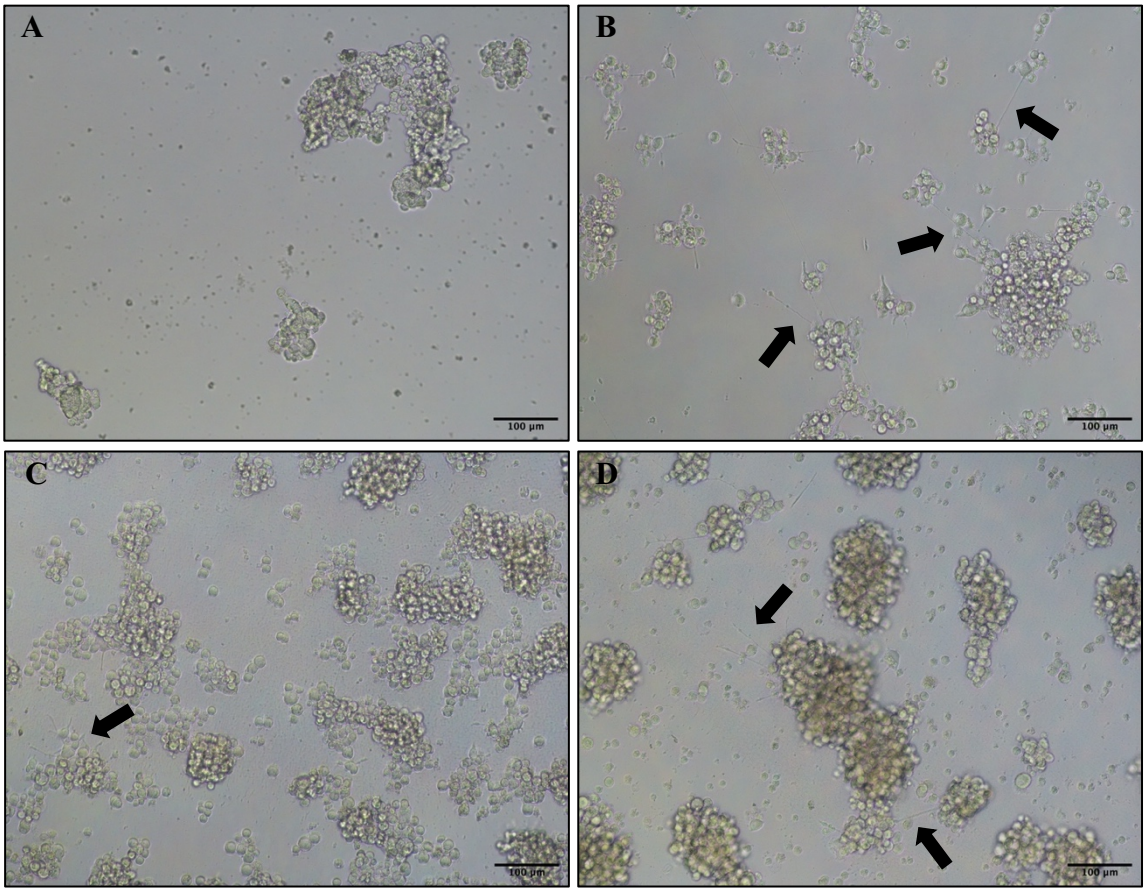

Figure 3.1: PC12 Cells Can Survive and Differentiate into Neuron-Like Cells on N_BSilk Films. The ability for N_BSilk to promote nerve growth was assessed using a neurite outgrowth assay. PC12 cells were seeded on either collagen or N_BSilk. The silk was provided with either NGF-L, NGF-M, both, or had no NGF present. Cell growth and neurite extension was monitored through optical analysis of 10 X bright field microscopy images. Data were collected from a single experiment with 4 internal replicates for each condition. Image **A)** shows the negative control at day 4 where cells were seeded on collagen, but received no NGF. Image **B)** shows the positive control at day 4 where cells were seeded on collagen + NGF-M. Image **C)** shows cells seeded on N_BSilk + NGF-L and NGF-M at day 4, and image **D)** shows the same condition at day 7 of culture. Black arrows highlight high neurite density in images, where applicable.

The bright field images from this cell culture experiment were quantified to compare both the density of neurites and the length of neurites that were observed in each condition. To also compare the metabolic state of the cells grown in each condition, a cell viability assay was conducted on the final day of cell culture. This type of assay requires

cell lysis to release ATP, which can be measured via luminescence. ATP content is a proxy for metabolic activity and has been widely used to examine overall cell viability (Riss *et al.,* 2004). Furthermore, the shift of cells from a proliferative state to a differentiative state has been shown to reflect changes in ATP content (Ataullakhanov and Vitvvitsky, 2002). For this experiment, I was more interested in observing changes in ATP content in cells that were exposed to NGF, compared to those that were not, as this would be further indicative of a metabolic shift associated with cellular differentiation, in addition to morphological features such as neurite extension.

Figure 3.2 A shows a shift in ATP content measured from cells cultured on silk conditions that received NGF-M, compared to their respective conditions that did not receive NGF-M; however, this trend did not apply to cells grown on collagen. A higher luminescent signal in both collagen conditions compared to all other conditions suggests more viable cells overall. This is to be expected, as PC12 cells typically require collagen substrates for cell culture (Wiatrak *et al,* 2020).

Interestingly, in conditions where neurite outgrowth was not observed optically, such as with cells grown on N_BSilk + NGF-L only, a large shift in ATP content was observed through this assay. I hypothesize that this is due to changes in cellular metabolism following signalling by NGF-L. Although these cells did not display morphological features of differentiation, this could have been due to the lack of cellular adherence to the silk substrate, while the cells growing in suspension could still have been signaling through NGF-induced signal transduction cascades.

When the neurite outgrowth data was quantified I observed a consistently low density of neurites of cells grown on silk compared to the positive control (Figure 3.2 B).

This was contradicting to other optical observations, such as the cells grown on N_BSilk + NGF-M and N_BSilk + NGF-M and NGF-L, did not appear to be in suspension, which would be more inhibitory to neurite outgrowth. It is possible that cells cultured on theN_BSilk were only able to achieve moderate adhesion to their substrate, compared to those grown on collagen, resulting in limited stability, which is required for neurite extension (Fuji *et al.,* 1982).

Notably, the few neurites that did extend on N_BSilk + NGF-M and NGF-L grew longer on average than those that extended from cells grown on collagen. This may be due to the greater concentration of NGF present in the N_BSilk + NGF-M and NGF-L cell culture condition; however, if that were the case, I would have also expected the N_BSilk + NGF-L condition to extend neurites, which it did not. Thus, it is possible that the presentation of NGF from N_BSilk enhanced the ability for neurites to continue extending over time. In natural biological systems, the ECM is able to control growth factor presentation to cells by binding and/or trapping molecules in its 3D matrix. This regulates growth factor signalling such that an appropriately sustained signal transduction can occur, as opposed to exposing cells to high concentrations of growth factors all at once (Lee *et al.,* 2011). These findings have prompted the engineering of biomaterials including polymers and fusion proteins that can immobilize growth factors, similar to the design of N_BSilk, to allow for a more sustained growth factor release which is largely dependent on the degradation of the material (Ren *et al.,* 2020).

Lastly, to ensure that the quantification of average neurite length was not limited by new neurites that were beginning to extend each day, the maximum neurite length was also analyzed in Figure 3.2 D. As the maximum neurite length continues to increase over

time, this indicates that individual neurites are continuing to lengthen each day. The maximum neurite length of cells grown on collagen increases in a linear fashion, whereas cells grown on N_BSilk when exposed to both NGF-M and NGF-L exhibited neurites that grew at a faster rate, albeit a much lower density.

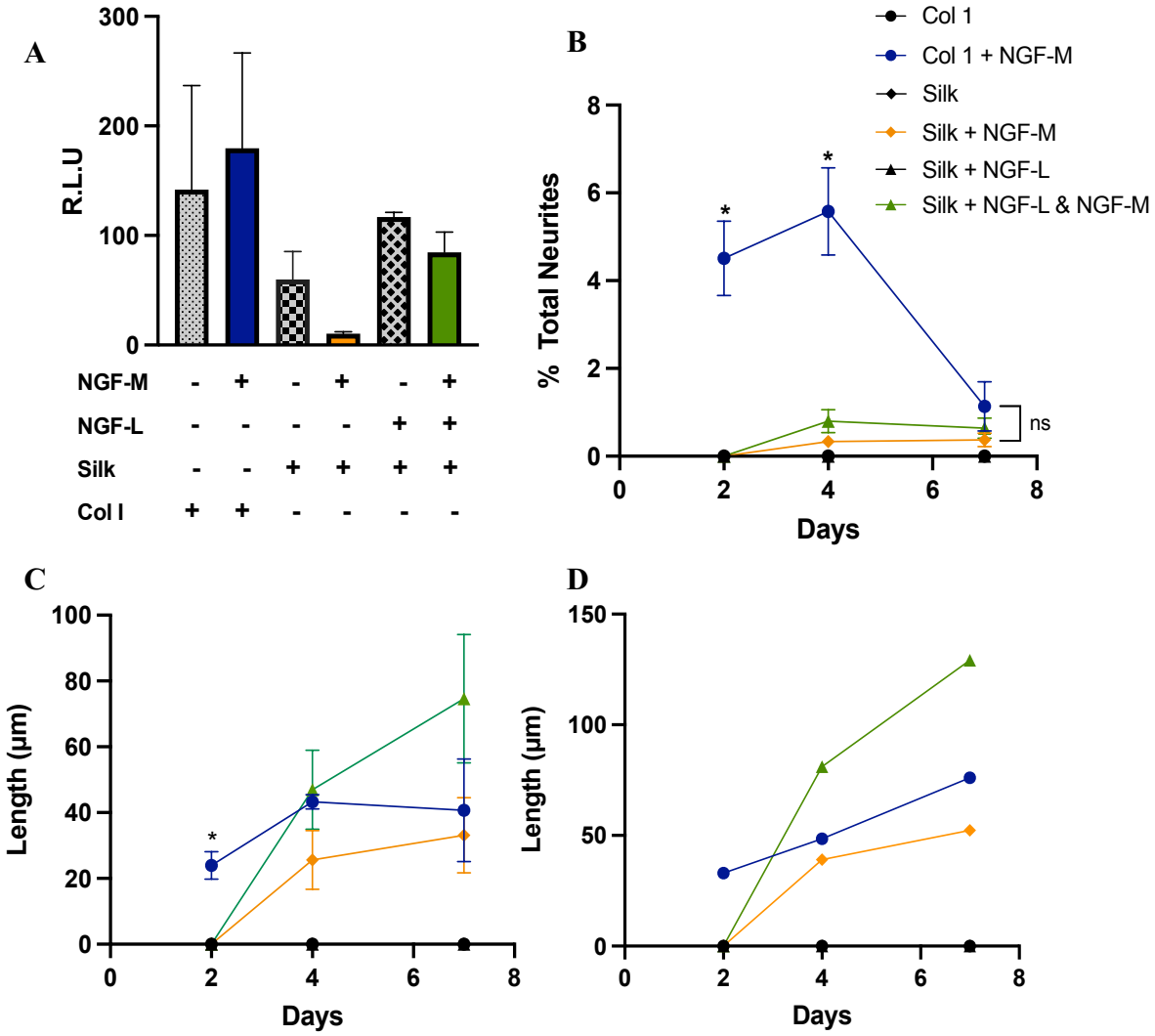

Figure 3.2: PC12 Cells Differentiate and Extend Few, but long Neurites when Cultured on N_BSilk. Following the neurite outgrowth assay described in section 3.2.2, optical images were analyzed using Image J and Neuron J to quantify neurite outgrowth. Panel **A)** shows ATP content measured as R.L.U from day 7 of each cell culture condition, determined by the CellTiter assay. Panel **B)** shows the density of neurites in conditions over the 7 day cell culture experiment. Panel **C)** shows the average length of neurites over the 7 days of cell culture, whereas panel **D)** shows the absolute maximum neurite length observed from each day in each condition. The legend for all figures is shown in the upper right of panel **B.** Data from a single experiment with 4 internal replicates for each condition were plotted as the mean +/- SEM and analyzed statistically with a 2-way ANOVA and Tukey's multiple comparison testing using GraphPad Prism 9. * = p-value < 0.05. Key non-significant findings are labelled "ns".

3.3.2: PC12 Adh Neurite Outgrowth Assay

Following the initial PC12 cell culture experiments, I also wanted investigate neurite outgrowth in a cell line with better adherence to a variety of substrates. Although traditional PC12 cells have been well characterized in their direct response to NGF, making them a good candidate as a model system to study N_BSilk *in vitro,* they require very specific cell culture coatings and conditions for optimal neurite extension. As neurite outgrowth is not only triggered by neurotrophin signaling, but also by cellular adhesion, repeating cell culture experiments with PC12 Adh cells to control for the variable of adherence was investigated next.

The same cell culture conditions were analyzed for this experiment; however, since the cells are adherent, no collagen coating is required for the positive and negative controls. PC12 Adh cells that were cultured directly on the tissue culture plate (TCP) with no NGF exposure had a basal level of differentiation and neurite outgrowth due to signaling that may have been directly from the adhesion. This was observed throughout the experiment, until day 7, when cells began to appear to apoptose due to a lack of survival signaling. Figure 3.3 A shows the negative control at the end of the cell culture experiment, where I observed morphological evidence of apoptosis, such as cell shrinkage and membrane blebbing (Saraste and Pulkki, 2000).

Cell adhesion molecules (CAMs) and ECM glycoproteins have been widely studied, in addition to growth factors, for their ability to stimulate neurite outgrowth (Bixby and Jhabvala, 1990). They stimulate differentiation by both mechanical guidance and triggering signal transduction cascades. CAMs, such as cadherins, interact with intracellular catenins to mediate arrangement of the cytoskeleton. Other CAMs, such as

L1-CAM and neural cell adhesion molecule (NCAM) were found to participate in interactions with ECM components (Kiryushko *et al.,*2004). Neuritogenesis is not only attributed to directional and guidance cues from these molecules associating with the ECM, but also intracellular signaling through the cAMP response element binding protein (CREB). This signaling ultimately results in the activation of transcription factors responsible for cell morphology changes in the CNS, including neurite extension (Lonze and Giny, 2002).

A key difference in this experiment, compared to that of the traditional PC12 cells, was the immediate and long-lasting neurite outgrowth observed in cells cultured on all N_BSilk conditions. Optically, the cells grown on N_BSilk displayed a high density of long neurites, similar to the positive control. Notably, cells grown on N_BSilk + NGF-L extended neurites, which is in contrast with results of the traditional PC12 cells grown in the same condition. This key finding suggests that N_BSilk itself may have an effect on cells, and neurite outgrowth of cells on this substrate is not dependent on NGF-M alone. Furthermore, this suggests that the NGF preloaded onto N_BSilk preceding cell seeding remains available to cells and in bioactive form.

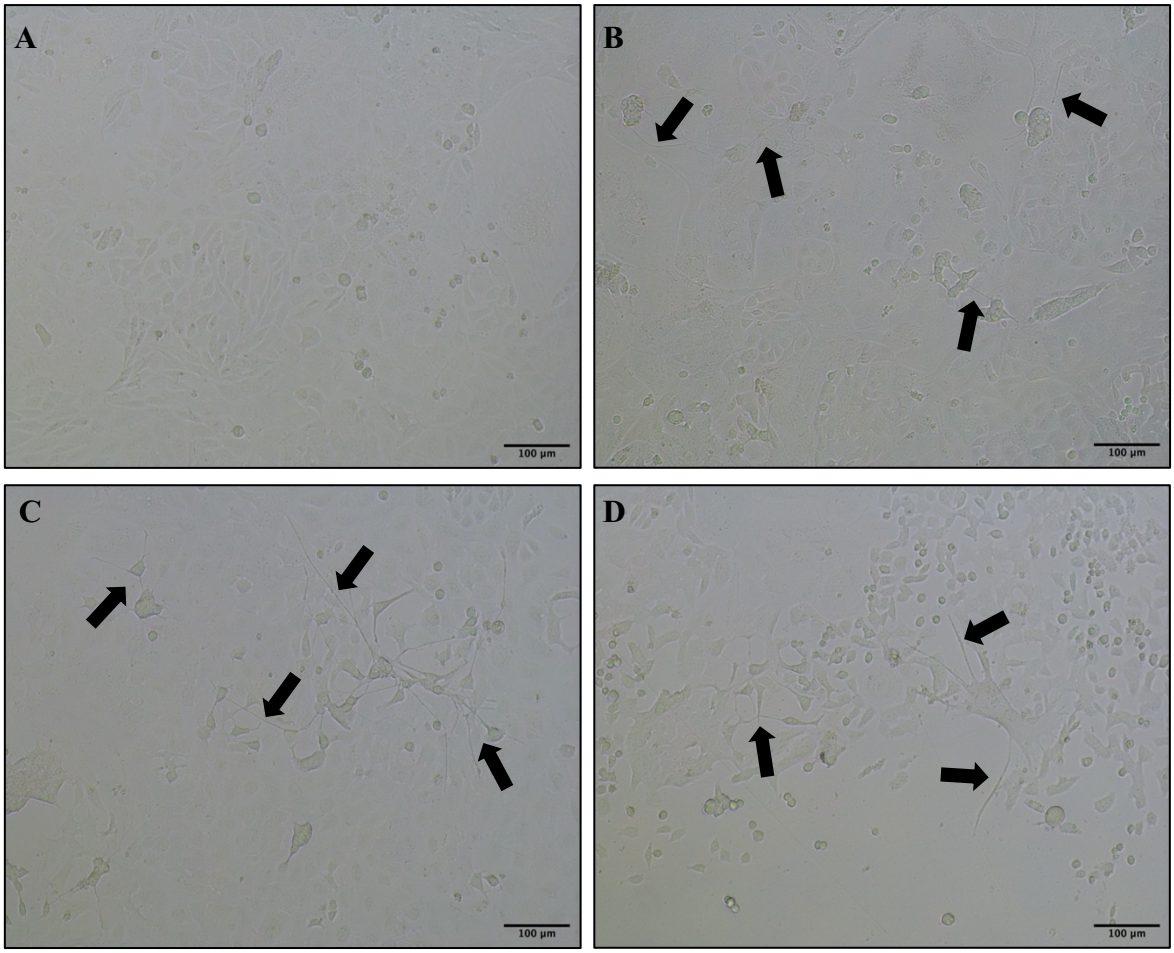

Figure 3.3: **PC12 Adh Cells Immediately Extend Neurites on N_BSilk.** The ability for N_BSilk to promote nerve growth was assessed using a neurite outgrowth assay. PC12 Adh cells were seeded on either the TCP or N_BSilk. The silk was either exposed to NGF-L, NGF-M, both or neither. Cell growth and neurite extension was monitored through optical analysis of 10 X bright field microscopy images. Data were collected from a single experiment with 4 internal replicates of each condition. Image **A)** shows the negative control at day 7 where cells were seeded on the TCP and received no NGF. Image **B)** shows the positive control at day 7 where cells were seeded on the TCP + NGF-M. Image **C)** shows cells seeded on N_BSilk +NGF-L at day 7. Image **D)** shows cells seeded on N_BSilk + NGF-L and NGF-M at day 7. Black arrows highlight high neurite density in images, where applicable.

When the cell viability assay was conducted with PC12 Adh cells following this experiment, the luminescent signal detected from ATP content was much more consistent across all groups, shown in Figure 3.4 A. An explanation for this result could be the higher level of cellular adhesion to both the TCP and N_BSilk, inherent to the cell line,

which allows for a higher basal level of differentiation and survival across groups, even the negative controls that did not receive NGF. This is further reflected with respect to neurite density, shown in Figure 3.4 B. The negative controls of cells cultured on the TCP or N_BSilk, that did not receive NGF, had consistent and similarly low densities of neurites over the week of cell culture. Neurite density of all other groups increased over time, with cells grown on silk displaying similar or even higher percentages of neurites per field of view than on the TCP. Moreover, cells grown on N_BSilk + NGF-L or N_BSilk + NGF-L and NGF-M continued to increase the density of neurites over time, whereas neurite density of other conditions began to decrease or plateau over time. This suggests a more sustained release of NGF from N_BSilk over time, which could allow the cells to continue neurite extension.

The length of neurites, shown in Figure 3.4 C, was very similar in all conditions until day 7, when the negative controls started to cease neurite extension. Through optical microscopy assessment of cell morphology, I observed cellular shrinkage and membrane blebbing in the negative control conditions. These morphological observations are often associated with apoptosis (Saraste and Pulkki, 2000), which may be the cause for retraction of neurites and cell death in these conditions.

The maximum length of neurites, shown in Figure 3.4 D, remained stable overtime across all groups, indicating more *de novo* neurite extension along with the continued lengthening from previously extended neurites. This is different from PC12 cells which exhibited less overall neurites being extended over time, but those that did initially extend, continued to grow longer with time. The steady decrease of maximum neurite length observed in the silk negative control is further indicative of no new

neurites being extended over time, while current or previously extended neurites began to break or retract with cell death. This result is to be expected over time with the negative controls, since cells are not receiving survival or differentiation signaling from NGF.

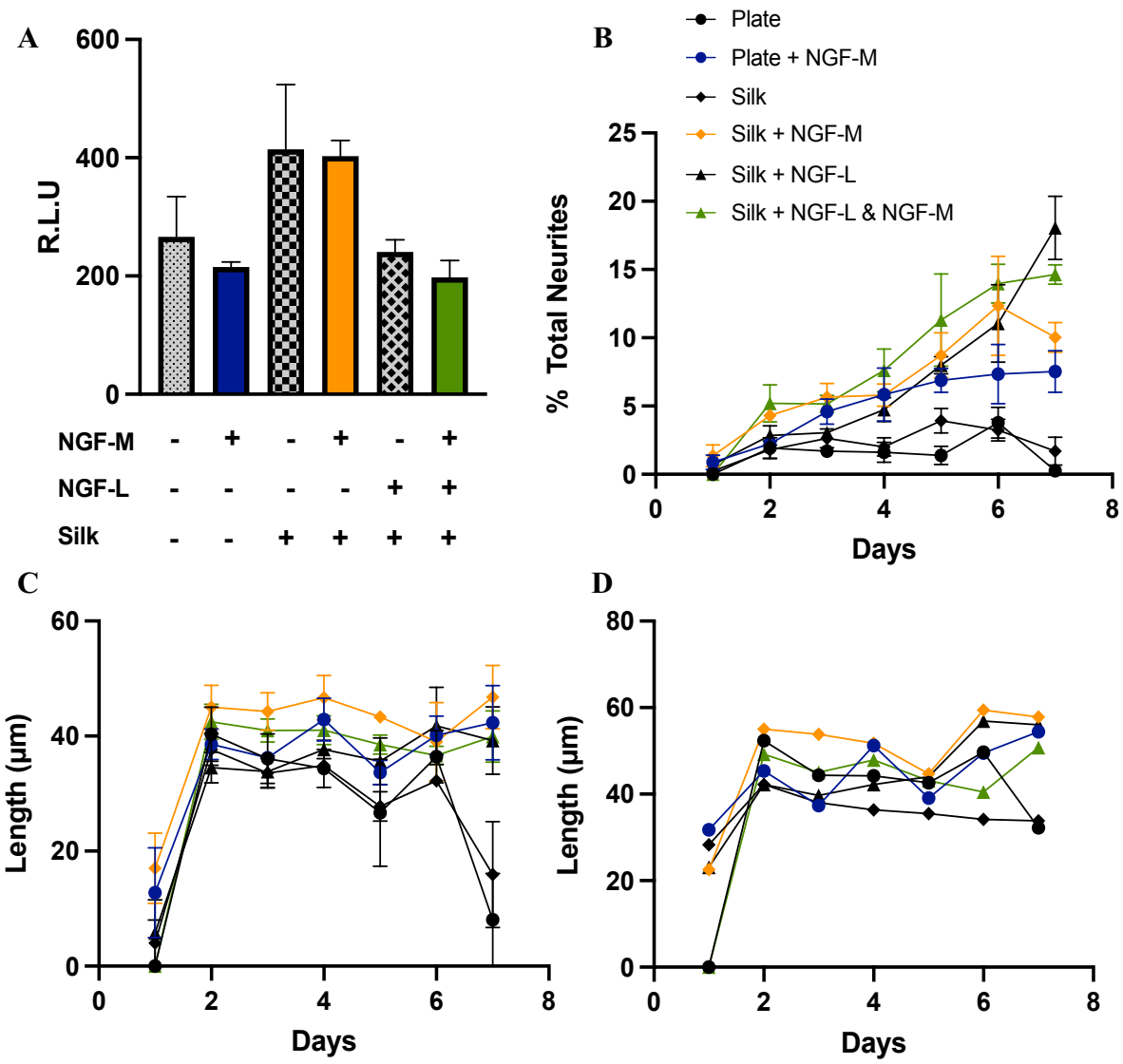

Figure 3.4: N_BSilk Enhances PC12 Adh Neurite Outgrowth. Following the neurite outgrowth assay described in section 3.2.2, optical images were analyzed using Image J and Neuron J to quantify neurite outgrowth. Panel **A)** shows ATP content measured as R.L.U from day 7 of each cell culture condition, determined by the CellTiter assay. Panel **B)** shows the density of neurites in conditions over the 7 day cell culture experiment. Panel **C)** shows the average length of neurites over the 7 days of cell culture, whereas panel **D)** shows the maximum neurite length. The legend for all figures is shown in the upper left of panel **B.** Data were plotted from single experiment with 4 internal replicates as the mean +/- SEM using GraphPad Prism 9.

The differences in neurite density and length between PC12 Adh cell culture conditions became more prominent on day 7, so I analyzed this day independently and compare each parameter across the different conditions. Figure 3.5 A shows the statistical comparison of neurite density in PC12 Adh cells on day 7 of cell culture, while Figure 3.5 B shows the comparison of neurite length. The main statistical differences are highlighted in the figures; however, all p-values for multiple comparisons can be found in Table A2. Most notably, the neurite density of both preloaded silk conditions was significantly greater than that of the positive control, thus indicating PC12 Adh cells preferred N_BSilk as a substrate for neurite extension over the TCP. Furthermore, there was no significant difference observed in neurite density from cells grown on N_BSilk + NGF-M and NGF-L, compared to N_BSilk + NGF-L only. This further supports that NGF preloaded onto N_BSilk is bioactive. Similarly, the length of neurites for both preloaded silk conditions did not differ significantly from each other; however in this case, both were also comparable to the positive control.

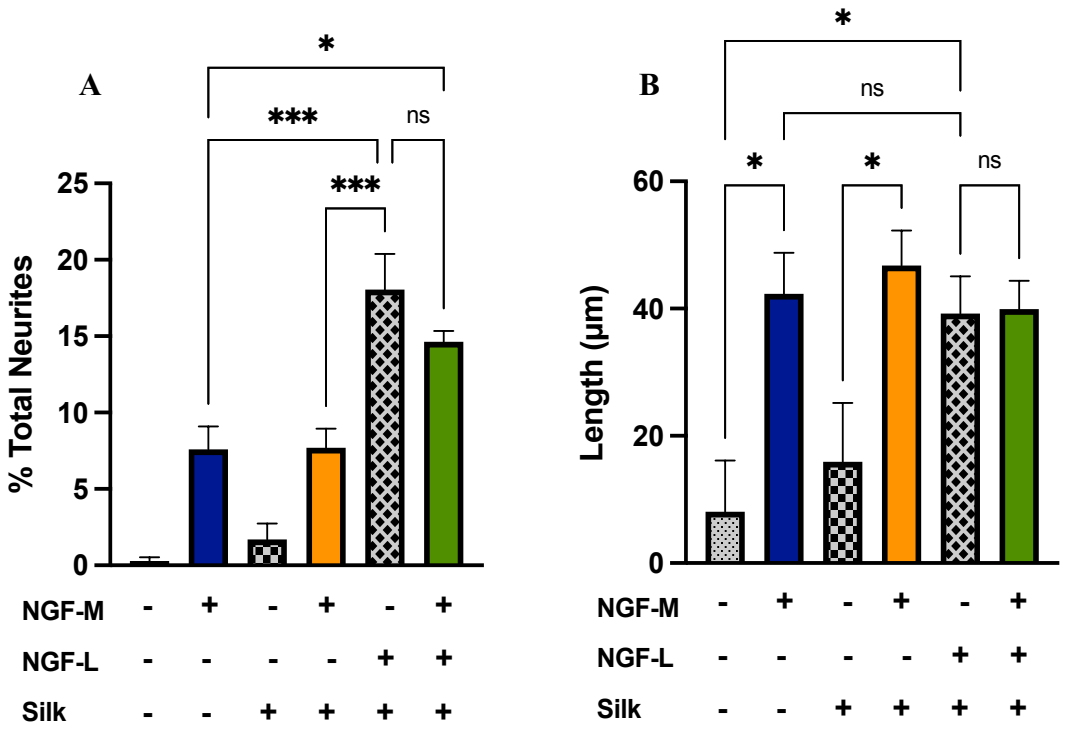

Figure 3.5: Statistical Analysis of PC12 Adh Cell Culture Data from Day 7 Reveals N_BSilk is a Preferred Substrate for Neurite Outgrowth. Following the neurite outgrowth assay, optical images were analyzed using Image J and Neuron J to quantify neurite outgrowth. Data from a single experiment with 4 internal replicates of each condition were plotted as the mean +/- SEM using GraphPad Prism 9. The previously shown data from Figure 3.4 B and C were analyzed statistically using an ANOVA and Tukey's multiple comparison testing to further show key differences from day 7 of cell culture. Panel **A)** shows neurite density from day 7 and panel **B)** shows neurite length from day 7. * = p-value < 0.05. *** = p-value < 0.0005. Key non-significant findings are labelled "ns".

3.3.3: Western Blot Analysis of PC12 Markers of NGF Signalling

To further investigate the finding that preloaded NGF on N_BSilk was directly having an effect on cells and inducing differentiation, I decided to probe for molecular markers of NGF-induced signaling in both PC12 and PC12 Adh cells. As discussed in section 3.1.1, NGF stimulates neurite outgrowth primarily through the MAPK pathway which leads to downstream phosphorylation of ERK1/2 by MEK, followed by the nuclear translocation of ERK1/2 to act on transcription factors that facilitate neurite outgrowth

(Klesse *et al.,* 1999). Other Ras-independent pathways have been involved in PC12 cell survival and differentiation, such as PI3-K signaling. Downstream phosphorylation of AKT is necessary in this pathway to induce cell survival mechanisms and prevent apoptosis, allowing subsequent differentiation (Ngyun *et al.,* 2010). Thus, the phosphorylation of ERK and AKT act as key markers of NGF-induced signal transduction through the TrkA receptor. I probed for phosphorylated AKT and ERK (pAKT, pERK) and non-phosphorylated AKT and ERK by western blotting, following cell incubation with NGF in the same conditions as with the neurite outgrowth assays in section 3.3.1 and 3.3.2.

Since traditional PC12 cells grown on N_BSilk + NGF-L did not extend neurites during the cell culture experiment in section 3.3.1, it remained unclear if N_BSilk was actually having an effect on cells itself, or if the neurite outgrowth observed in other conditions was from the NGF-M alone. Furthermore, the low density of neurites observed from cells grown on N_BSilk may have been due to poor adhesion to the substrate, while cellular differentiation signaling by NGF-L may have still occurred. Thus, examining the phosphorylation of AKT and ERK in response to NGF provided a non-optical, biochemical method to analyze NGF signalling at the molecular level within PC12 cells.

When pERK/ERK (Figure 3.6 A) and pAKT/AKT (Figure 3.6 B) in traditional PC12 cells was plotted, I observed higher phosphorylation ratios in all conditions that received NGF, either preloaded onto silk or in the culture medium. This is expected as these two pathways become activated upon stimulation by NGF through TrkA. I also observed pERK and pAKT on the immunoblots (representative blots shown above each plot in Figure 3.6) in the condition where cells were grown on N_BSilk + NGF-L only. No

neurites were observed optically in this condition during the neurite outgrowth assay, but results of this analysis indicate that signaling by NGF was still occurring. This finding suggests that the main hindrance of neurite outgrowth for traditional PC12 cells grown on N_BSilk was the lack of adhesion to the substrate that occurs with this model system. Furthermore, there was no significant difference in the ratio of either pAKT/AKT or pERK/ERK in PC12 cells grown on N_BSilk + NGF-L, N_BSilk + NGF-L and NGF-M, or collagen I and IV. This indicates a similar level of NGF-induced signaling in these conditions regardless of visible neurite outgrowth. P-values for all multiple comparisons can be observed in Table A1, as only those of interest were shown in Figure 3.6.

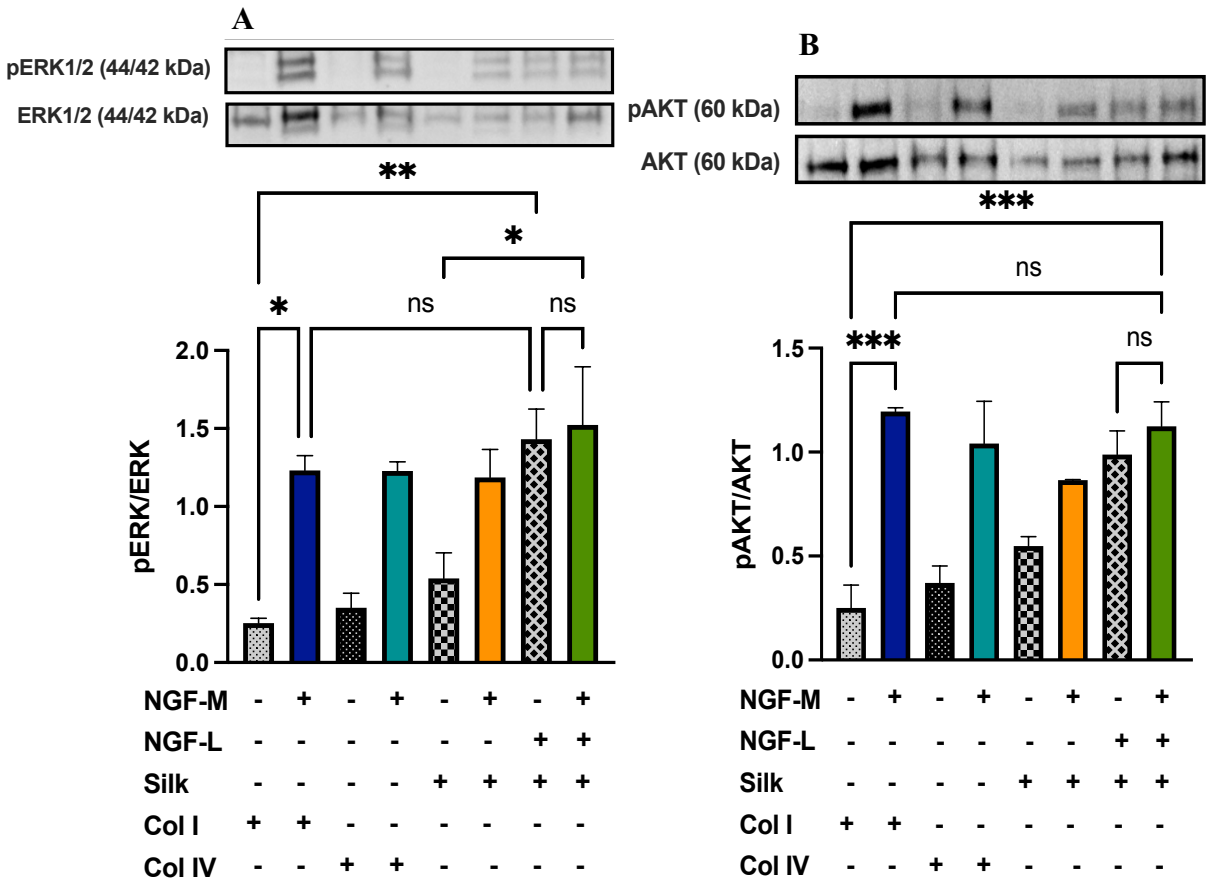

Figure 3.6: **NGF-Induced Phosphorylation of AKT and ERK in PC12 Cells Cultured on N_BSilk.** Cells were cultured for 30 min in conditions as described in section 3.2.6 to probe for protein markers of NGF-induced differentiation. Panel **A)** shows a representative blot for pERK and ERK, and the integrated density plotted as a ratio of pERK/ERK. Panel **B)** shows a representative blot for pAKT and AKT, and the integrated density plotted as a ratio of pAKT/AKT. Integrated density from blots was determined using Image J, then plotted as the mean ratio of phosphorylated protein to total protein, +/- SEM. Data from 3 individual experiments with 4 internal replicates of each condition were analyzed statistically with an ANOVA and Tukey's multiple comparison testing, using GraphPad Prism 9**.** * = p-value < 0.05. ** = p-value < 0.005. *** = p-value < 0.0005. Key non-significant findings are labelled "ns".

Similar trends were observed when the same proteins were probed for in PC12 Adh cells following induction by NGF. No significant difference was observed in pERK/ERK between N_BSilk conditions with NGF-L, shown in Figure 3.7 A. Although cells were exposed to both NGF-L and NGF-M in one condition, results of this

experiment indicate that it did not induce more MAPK signaling, compared to cell culture on N_BSilk + NGF-L only. This suggests that the presentation of NGF-L by N_BSilk could be preferred by PC12 cell lines, or more available than NGF-M. Both preloaded N_BSilk conditions were also comparable to the positive control of PC12 Adh cells cultured on the TCP, with respect to the level of pERK. Furthermore, the negative controls tended to have higher basal levels of pERK, but conditions exposed to NGF-L or NGF-M generally still had a significantly higher level of pERK than those that did not receive any NGF. The higher basal level of phosphorylation within PC12 Adh cells could be due to the adherent nature of this cell line, which contributes neurite extension in addition to NGF signalling (Bixby and Jhabvala, 1990).

With respect to pAKT shown in Figure 3.7 B, I observed similar amounts of pAKT overall, resulting in no significant differences between groups. The trend of increased AKT phosphorylation in N_BSilk + NGF-L was still present; however, more replicate experiments would need to be completed to observe any potential statistical differences. These results are consistent with the microscopy images with respect to cell survival, as all conditions were observed to have cells remaining by day 7 of culture. Signaling through AKT is mainly used to promote cell survival mechanisms, so I would expect a generally similar ratio of pAKT/AKT across all conditions, as cells for this experiment were incubated in their respective condition for only 30 min prior to cell lysis for western blot analysis. During the longer neurite outgrowth assay, PC12 Adh cells grown in negative control conditions remained viable until day 7 of cell culture. Therefore, the signaling these cells receive from adherence to the TCP or other substrate could be sufficient for initial cell survival in low-serum medium . Over time, they may

require additional signaling from growth factors, such as NGF, to maintain viability and differentiate.

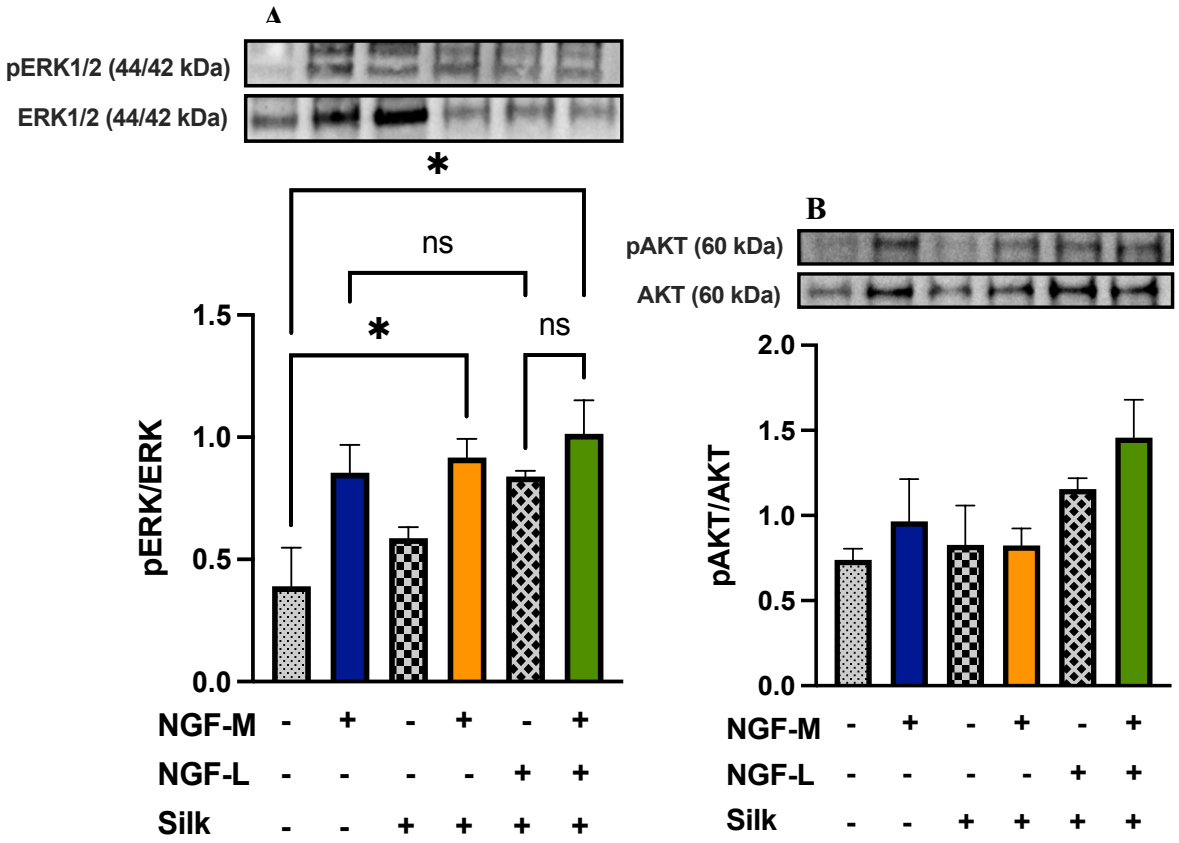

Figure 3.7: NGF-Induced Phosphorylation of AKT and ERK in PC12 Adh Cells Cultured on N_BSilk. Cells were cultured for 30 min in various conditions as described in section 3.2.6 to probe for protein markers of NGF-induced differentiation. Panel **A)** shows a representative blot for pERK and ERK, and the integrated density plotted as a ratio of pERK/ERK. Panel **B)** shows a representative blot for pAKT and AKT, and the integrated density plotted as a ratio of pAKT/AKT. Integrated density was determined from western blots using Image J, then plotted as the mean ratio of phosphorylated protein to total protein, +/- SEM. Data Data from 3 individual experiments with 4 internal replicates of each condition were analyzed statistically with an ANOVA and Tukey's multiple comparison testing, using GraphPad Prism 9**.** * = p-value < 0.05. Key non-significant findings are labelled "ns".

3.3.4: Conclusions

This chapter explored the bioactivity of NGF presented by N_BSilk using *in vitro* experiments with 2 unique PC12 cell lines. Optical microscopy analysis indicated that traditional PC12 cells appeared to be able to survive and differentiate on N_BSilk, however they required both NGF-L and NGF-M for optimal neurite outgrowth, which remained at a low density compared to cells grown on collagen. Neurites that did extend from cells on N_BSilk continued to grow in length over time. The cells that did not extend neurites on N_BSilk in other cell culture conditions could still signaling through NGF-induced transduction pathways, but were unable to extend neurites due to the poor adhesion of this cell line to substrates. This was hypothesized following western blot analysis of NGF-signalling targets, pERK and pAKT, which were found at significantly greater levels in PC12 cells grown on N_BSilk + NGF-L, compared to cells grown on collagen.

To control for the variable of cell adhesion preferences to specific substrates, PC12 Adh cells were also cultured and analyzed for neurite outgrowth. These cells extended a high density of neurites on all N_BSilk conditions for the duration of the experiment, with a significantly greater number of neurites than cells grown on the TCP, by day 7 of culture. The length of neurites extended on silk was also comparable to those on the TCP + NGF-M for the duration of the experiment. The differences between NGF-signalling targets in PC12 Adh cells were much less distinct between conditions compared to traditional PC12 cells, due to the increased adhesion of the cells; however, overall, the same trends of increased pERK and pAKT relative to total ERK and AKT was observed in N_BSilk and TCP conditions exposed to NGF.

The discussed results indicate that N_BSilk is a suitable substrate for PC12 cell growth and differentiation, as the presentation of sequestered NGF-L was able to enhance neurite outgrowth and survival. This provides promising evidence for the use of N_BSilk as a biomaterial for neuronal growth. The future of N_BSilk for nerve regeneration applications will be discussed at greater length and summarized in Chapter 4.

Chapter 4: Conclusion

4.1: Summary

During this project I was able to produce the recombinant aciniform silk construct, N_BSilk, and test its ability as a biomaterial for nerve growth. I developed appropriate expression and purification protocols for N_BSilk that can be implemented for other recombinant aciniform constructs in the future. The lyophilized protein was successfully suspended in a TFA:TFE:H_2O solvent that is appropriate for both film-casting and fibre wet-spinning. The N_BSilk suspension was cast into protein films suitable for silk characterization and cell culture experiments. By developing a custom ELISA protocol to assess the NGF-binding ability of N_BSilk, I was able to show that while the protein was in film form the NGF-binding motif was still available and able to sequester NGF at various concentrations. This suggested N_BSilk films were an appropriate substrate for cell culture. Furthermore, N_BSilk released NGF slowly over time and in small quantities compared to the amount that was initially loaded onto the film. In theory, this would limit off-target signaling of NGF in future *in vivo* models.

The ability for N_BSilk to enhance neuronal growth was assessed with 2 cell lines that differentiate into sympathetic-like neurons in response to induction by NGF. Both traditional PC12 and PC12 Adh cells were cultured on N_BSilk films in a variety of conditions to analyse its ability to promote survival and neurite outgrowth by either presenting preloaded or medium-sequestered NGF to cells. Traditional PC12 cells were able to survive and extend long neurites when cultured on the condition that presented both preloaded NGF, and NGF in the culture medium. Upon western blot analysis of traditional PC12 cells, it was found that cells cultured in the presence of preloaded NGF only were also being stimulated through the differentiation and survival pathways of

MAPK and PI3K. Conditions with PC12 Adh cells cultured on N_BSilk films preloaded with NGF only displayed the ability to induce neurite outgrowth significantly greater than the positive control, and this was further confirmed by western blot analysis indicating induction of MAPK and PI3K pathways. The ability for both of these cell lines to survive and differentiate on N_BSilk suggest its biocompatibility as a substrate for neuronal growth. This is the first known recombinant aciniform silk bioengineered with binding domains for the neurotrophic factor, NGF. Our results suggest that this construct is a promising biomaterial for the development and study of novel therapeutic options for spinal cord injuries and other nerve regeneration applications.

4.2: Future Directions

Although these results proved to be exciting, future experiments should be conducted to better understand N_BSilk before moving forward with *in vivo* studies. A more in depth analysis of protein and film structure and would be helpful to better tailor N_BSilk for nerve growth. Deconvolution of the FTIR spectrum in Figure 2.6, and further biophysical analysis including atomic force microscopy, will elucidate the structure and topology of N_BSilk protein films. This is important as topological and structural features have been shown to be implicated in neurite extension and nerve regeneration (cheng *et al.,* 2014; Smeal *et al.,* 2005; Tsuruma *et al.,* 2006).

Furthermore, I would be interested in testing the fibre-forming ability of N_BSilk in the solvents selected for film-casting. Films have a wide potential for biomaterial applications, such as with device coatings, wound dressings, and drug delivery (Borker *et al.,* 2014); however, silk fibres are specifically of interest for their mechanical properties and ability to promote nerve guidance. Neurite extension from cells is an important

component of regeneration, but being able to provide directional cues so axons extend in an appropriate orientation is also key. It is perhaps possible to use protein films to create a gradient of preloaded NGF that could guide the neurite outgrowth. Fibres, however, inherently have a long and narrow structure, which could provide guidance cues as neurites extend over longer distances. Therefore, future work with N_BSilk should comprise of fibre-wet spinning, followed by an analysis of fibre secondary structure characteristics to determine if the NGF-binding motif affects the silk's ability to form fibres, or alters its mechanical properties compared to other recombinant W_2 constructs, lacking this domain. Following studies should include ELISA-based NGF-binding assays to determine if the binding motif remains available upon fibre formation. Similar studies with PC12 cells can be repeated with cells seeded onto fibres to determine their ability to promote and guide neuritogenesis. Overall, the results discussed in this dissemination warrant future studies for N_BSilk to determine its most appropriate use as a biomaterial for nerve regeneration applications.

Bibliography

Abcam (2018). ELISA guide.

Abe, N., and Cavalli, V. (2008). Nerve injury signaling. Current Opinion in Neurobiology *18*, 276–283.

Ahuja, C.S., Nori, S., Tetreault, L., Wilson, J., Kwon, B., Harrop, J., Choi, D., and Fehlings, M.G. (2017). Traumatic Spinal Cord Injury—Repair and Regeneration. Neurosurgery *80*, S9–S22.

Althagafi, A., and Nadi, M. (2021). Acute Nerve Injury. In StatPearls, (Treasure Island (FL): StatPearls Publishing).

Anton, E.S., Weskamp, G., Reichardt, L.F., and Matthew, W.D. (1994). Nerve growth factor and its low-affinity receptor promote Schwann cell migration. Proc Natl Acad Sci U S A *91*, 2795–2799.

Ataullakhanov, F.I., and Vitvitsky, V.M. (2002). What determines the intracellular ATP concentration. Biosci Rep *22*, 501–511.

Azbill, R.D., Mu, X., and Springer, J.E. (2000). Riluzole increases high-affinity glutamate uptake in rat spinal cord synaptosomes. Brain Res *871*, 175–180.

Baoyong, L., Jian, Z., Denglong, C., and Min, L. (2010). Evaluation of a new type of wound dressing made from recombinant spider silk protein using rat models. Burns *36*, 891–896.

Batchelor, P.E., Wills, T.E., Skeers, P., Battistuzzo, C.R., Macleod, M.R., Howells, D.W., and Sena, E.S. (2013). Meta-Analysis of Pre-Clinical Studies of Early Decompression in Acute Spinal Cord Injury: A Battle of Time and Pressure. PLOS ONE *8*, e72659.

Bibel, M., Hoppe, E., and Barde, Y.A. (1999). Biochemical and functional interactions between the neurotrophin receptors trk and p75NTR. EMBO J *18*, 616–622.

Bixby, J.L., and Jhabvala, P. (1990). Extracellular matrix molecules and cell adhesion molecules induce neurites through different mechanisms. Journal of Cell Biology *111*, 2725–2732.

Borkner, C.B., Elsner, M.B., and Scheibel, T. (2014). Coatings and Films Made of Silk Proteins. ACS Appl. Mater. Interfaces *6*, 15611–15625.

Bracken, M.B. (2012). Steroids for acute spinal cord injury. Cochrane Database Syst Rev *1*, CD001046.

von Büdingen, H.-C., Mei, F., Greenfield, A., Jahn, S., Shen, Y.-A.A., Reid, H.H., McKemy, D.D., and Chan, J.R. (2015). The myelin oligodendrocyte glycoprotein directly binds nerve growth factor to modulate central axon circuitry. J Cell Biol *210*, 891–898.

Burnett, M.G., and Zager, E.L. (2004). Pathophysiology of peripheral nerve injury: a brief review. Neurosurgical Focus *16*, 1–7.

Cafferty, W.B.J., Duffy, P., Huebner, E., and Strittmatter, S.M. (2010). MAG and OMgp synergize with Nogo-A to restrict axonal growth and neurological recovery after spinal cord trauma. J Neurosci *30*, 6825–6837.

Caillaud, M., Richard, L., Vallat, J.-M., Desmoulière, A., and Billet, F. (2019). Peripheral nerve regeneration and intraneural revascularization. Neural Regen Res *14*, 24–33.

Campbell, W.W. (2008). Evaluation and management of peripheral nerve injury. Clin Neurophysiol *119*, 1951–1965.

Cantile, C., and Youssef, S. (2016). Nervous System. Jubb, Kennedy & Palmer's Pathology of Domestic Animals: Volume 1 250–406.

Carvalho, C.R., Oliveira, J.M., and Reis, R.L. (2019). Modern Trends for Peripheral Nerve Repair and Regeneration: Beyond the Hollow Nerve Guidance Conduit. Front. Bioeng. Biotechnol. *7*.

Chandrasekaran, S., Davis, J., Bersch, I., Goldberg, G., and Gorgey, A.S. (2020). Electrical stimulation and denervated muscles after spinal cord injury. Neural Regen Res *15*, 1397–1407.

Chen, Y.-S., Wu, C.-H., Yao, C.-H., and Chen, C.-T. (2002). Ginsenoside Rb1 Enhances Peripheral Nerve Regeneration across Wide Gaps in Silicone Rubber Chambers. Int J Artif Organs *25*, 1103–1108.

Chen, Z.-L., Yu, W.-M., and Strickland, S. (2007). Peripheral Regeneration. Annual Review of Neuroscience *30*, 209–233.

Cheng, H., Zhou, L., Li, B., Zhu, M., Too, H.-P., and Choi, W.K. (2014). Nano-topology guided neurite outgrowth in PC12 cells is mediated by miRNAs. Nanomedicine: Nanotechnology, Biology and Medicine *10*, 1871–1875.

Christensen, M.D., and Hulsebosch, C.E. (1997). Chronic central pain after spinal cord injury. J Neurotrauma *14*, 517–537.

Costa, S., Almeida, A., Castro, A., and Domingues, L. (2014). Fusion tags for protein solubility, purification and immunogenicity in Escherichia coli: the novel Fh8 system. Front. Microbiol. *0*.

Davies, A.M. (1994). The role of neurotrophins in the developing nervous system. Journal of Neurobiology *25*, 1334–1348.

Delfino, I., Portaccio, M., Ventura, B.D., Mita, D.G., and Lepore, M. (2013). Enzyme distribution and secondary structure of sol–gel immobilized glucose oxidase by micro-attenuated total reflection FT-IR spectroscopy. Materials Science and Engineering: C *33*, 304–310.

Faroni, A., Mobasseri, S.A., Kingham, P.J., and Reid, A.J. (2015). Peripheral nerve regeneration: experimental strategies and future perspectives. Adv Drug Deliv Rev *82–83*, 160–167.

Fehlings, M.G., Theodore, N., Harrop, J., Maurais, G., Kuntz, C., Shaffrey, C.I., Kwon, B.K., Chapman, J., Yee, A., Tighe, A., et al. (2011). A phase I/IIa clinical trial of a recombinant Rho protein antagonist in acute spinal cord injury. J Neurotrauma *28*, 787–796.

Fine, E.G., Decosterd, I., Papaloïzos, M., Zurn, A.D., and Aebischer, P. (2002). GDNF and NGF released by synthetic guidance channels support sciatic nerve regeneration across a long gap. Eur J Neurosci *15*, 589–601.

Fricker, M., Tolkovsky, A.M., Borutaite, V., Coleman, M., and Brown, G.C. (2018). Neuronal Cell Death. Physiol Rev *98*, 813–880.

Frostick, S.P., Yin, Q., and Kemp, G.J. (1998). Schwann cells, neurotrophic factors, and peripheral nerve regeneration. Microsurgery *18*, 397–405.

Fujii, D.K., Massoglia, S.L., Savion, N., and Gospodarowicz, D. (1982). Neurite outgrowth and protein synthesis by PC12 cells as a function of substratum and nerve growth factor. J Neurosci *2*, 1157–1175.

Greene, L.A., and Tischler, A.S. (1976). Establishment of a noradrenergic clonal line of rat adrenal pheochromocytoma cells which respond to nerve growth factor. Proc Natl Acad Sci U S A *73*, 2424–2428.

Hayashi, C.Y., and Lewis, R.V. (1998). Evidence from flagelliform silk cDNA for the structural basis of elasticity and modular nature of spider silks. J Mol Biol *275*, 773–784.

Hayashi, C.Y., Blackledge, T.A., and Lewis, R.V. (2004a). Molecular and mechanical characterization of aciniform silk: uniformity of iterated sequence modules in a novel member of the spider silk fibroin gene family. Mol Biol Evol *21*, 1950–1959.

Heidebrecht, A., and Scheibel, T. (2013). Recombinant production of spider silk proteins. Adv Appl Microbiol *82*, 115–153.

Hennecke, K., Redeker, J., Kuhbier, J.W., Strauss, S., Allmeling, C., Kasper, C., Reimers, K., and Vogt, P.M. (2013a). Bundles of Spider Silk, Braided into Sutures, Resist Basic Cyclic Tests: Potential Use for Flexor Tendon Repair. PLoS One *8*, e61100.

Hennecke, K., Redeker, J., Kuhbier, J.W., Strauss, S., Allmeling, C., Kasper, C., Reimers, K., and Vogt, P.M. (2013b). Bundles of Spider Silk, Braided into Sutures, Resist Basic Cyclic Tests: Potential Use for Flexor Tendon Repair. PLoS One *8*, e61100.

Higuchi, M., Onishi, K., Masuyama, N., and Gotoh, Y. (2003). The phosphatidylinositol-3 kinase (PI3K)-Akt pathway suppresses neurite branch formation in NGF-treated PC12 cells. Genes Cells *8*, 657–669.

Higuchi, M., Onishi, K., Kikuchi, C., and Gotoh, Y. (2008). Scaffolding function of PAK in the PDK1–Akt pathway. Nat Cell Biol *10*, 1356–1364.
Hinman, M.B., Jones, J.A., and Lewis, R.V. (2000). Synthetic spider silk: a modular fiber. Trends in Biotechnology *18*, 374–379.

Holland, C., Numata, K., Rnjak-Kovacina, J., and Seib, F.P. (2019). The Biomedical Use of Silk: Past, Present, Future. Advanced Healthcare Materials *8*, 1800465.

Huebner, E.A., and Strittmatter, S.M. (2009). Axon Regeneration in the Peripheral and Central Nervous Systems. Results Probl Cell Differ *48*, 339–351.

Huemmerich, D., Helsen, C.W., Quedzuweit, S., Oschmann, J., Rudolph, R., and Scheibel, T. (2004). Primary structure elements of spider dragline silks and their contribution to protein solubility. Biochemistry *43*, 13604–13612.

Jing, S., Tapley, P., and Barbacid, M. (1992). Nerve growth factor mediates signal transduction through trk homodimer receptors. Neuron *9*, 1067–1079.

Kato, S., Matsukawa, T., Koriyama, Y., Sugitani, K., and Ogai, K. (2013). A molecular mechanism of optic nerve regeneration in fish: The retinoid signaling pathway. Progress in Retinal and Eye Research *37*, 13–30.

Kehoe, S., Zhang, X.F., and Boyd, D. (2012). FDA approved guidance conduits and wraps for peripheral nerve injury: a review of materials and efficacy. Injury *43*, 553–572.

Kim, Y., Seger, R., Suresh Babu, C.V., Hwang, S.-Y., and Yoo, Y.S. (2004). A positive role of the PI3-K/Akt signaling pathway in PC12 cell differentiation. Mol Cells *18*, 353–359.

Kiryushko, D., Berezin, V., and Bock, E. (2004). Regulators of neurite outgrowth: role of cell adhesion molecules. Ann N Y Acad Sci *1014*, 140–154.

Kiseleva, A.P., Krivoshapkin, P.V., and Krivoshapkina, E.F. (2020). Recent Advances in Development of Functional Spider Silk-Based Hybrid Materials. Front. Chem. *8*.

Klesse, L.J., Meyers, K.A., Marshall, C.J., and Parada, L.F. (1999). Nerve growth factor induces survival and differentiation through two distinct signaling cascades in PC12 cells. Oncogene *18*, 2055–2068.

Kornfeld, T., Nessler, J., Helmer, C., Hannemann, R., Waldmann, K.H., Peck, C.T., Hoffmann, P., Brandes, G., Vogt, P.M., and Radtke, C. (2021). Spider silk nerve graft promotes axonal regeneration on long distance nerve defect in a sheep model. Biomaterials *271*, 120692.

Kramer, J.P.M., Aigner, T.B., Petzold, J., Roshanbinfar, K., Scheibel, T., and Engel, F.B. (2020). Recombinant spider silk protein eADF4(C16)-RGD coatings are suitable for cardiac tissue engineering. Sci Rep *10*, 8789.

Kremer, N.E., D'Arcangelo, G., Thomas, S.M., DeMarco, M., Brugge, J.S., and Halegoua, S. (1991). Signal transduction by nerve growth factor and fibroblast growth factor in PC12 cells requires a sequence of src and ras actions. J Cell Biol *115*, 809–819.

Krenz, N.R., and Weaver, L.C. (2000). Nerve growth factor in glia and inflammatory cells of the injured rat spinal cord. J Neurochem *74*, 730–739.

Krenz, N.R., Meakin, S.O., Krassioukov, A.V., and Weaver, L.C. (1999). Neutralizing intraspinal nerve growth factor blocks autonomic dysreflexia caused by spinal cord injury. J Neurosci *19*, 7405–7414.

Leal-Egaña, A., and Scheibel, T. (2010). Silk-based materials for biomedical applications. Biotechnol Appl Biochem *55*, 155–167.

Lee, K., Silva, E.A., and Mooney, D.J. (2011). Growth factor delivery-based tissue engineering: general approaches and a review of recent developments. J R Soc Interface *8*, 153–170.

Lee, S.K., and Wolfe, S.W. (2000). Peripheral Nerve Injury and Repair. JAAOS - Journal of the American Academy of Orthopaedic Surgeons *8*, 243–252.

Lewis, R.V. (2006). Spider Silk: Ancient Ideas for New Biomaterials. Chem. Rev. *106*, 3762–3774.

Lonze, B.E., and Ginty, D.D. (2002). Function and regulation of CREB family transcription factors in the nervous system. Neuron *35*, 605–623.

MacInnis, B.L., and Campenot, R.B. (2002). Retrograde support of neuronal survival without retrograde transport of nerve growth factor. Science *295*, 1536–1539.

Makwana, M., and Raivich, G. (2005). Molecular mechanisms in successful peripheral regeneration. The FEBS Journal *272*, 2628–2638.

Meijering, E., Jacob, M., Sarria, J.-C.F., Steiner, P., Hirling, H., and Unser, M. (2004). Design and validation of a tool for neurite tracing and analysis in fluorescence microscopy images. Cytometry *58A*, 167–176.

Millesi, F., Weiss, T., Mann, A., Haertinger, M., Semmler, L., Supper, P., Pils, D., Naghilou, A., and Radtke, C. (2021). Defining the regenerative effects of native spider silk fibers on primary Schwann cells, sensory neurons, and nerve-associated fibroblasts. The FASEB Journal *35*, e21196.

Mirsky, R., and Jessen, K.R. (1999). The Neurobiology of Schwann Cells. Brain Pathology *9*, 293–311.

Murakami, Y., Furukawa, S., Nitta, A., and Furukawa, Y. (2002). Accumulation of nerve growth factor protein at both rostral and caudal stumps in the transected rat spinal cord. J Neurol Sci *198*, 63–69.

Nguyen, T.L., Kim, C.K., Cho, J.-H., Lee, K.-H., and Ahn, J.-Y. (2010). Neuroprotection signaling pathway of nerve growth factor and brain-derived neurotrophic factor against staurosporine induced apoptosis in hippocampal H19-7 cells. Exp Mol Med *42*, 583–595.

Nova, A., Keten, S., Pugno, N.M., Redaelli, A., and Buehler, M.J. (2010). Molecular and Nanostructural Mechanisms of Deformation, Strength and Toughness of Spider Silk Fibrils. Nano Lett. *10*, 2626–2634.
Okur, Z., Senturk, O.I., Yilmaz, C., Gulseren, G., Mammadov, B., Guler, M.O., and Tekinay, A.B. (2018). Promotion of neurite outgrowth by rationally designed NGF-β binding peptide nanofibers. Biomater. Sci. *6*, 1777–1790.

Perera, P.G.T., Bazaka, O., Bazaka, K., Appadoo, D., Croft, R.J., Crawford, R.J., and Ivanova, E.P. (2019). Pheochromocytoma (PC 12) as a Model Cell Line for Membrane Permeabilization Studies in the presence of Electromagnetic Fields (EMFs): Recent Advances. Journal of Neurology & Neuromedicine *4*.

Rasmussen, J.P., and Sagasti, A. (2017). Learning to swim, again: Axon regeneration in fish. Experimental Neurology *287*, 318–330.

Ren, X., Zhao, M., Lash, B., Martino, M.M., and Julier, Z. (2020). Growth Factor Engineering Strategies for Regenerative Medicine Applications. Front. Bioeng. Biotechnol. *0*.

Richner, M., Ulrichsen, M., Elmegaard, S.L., Dieu, R., Pallesen, L.T., and Vaegter, C.B. (2014). Peripheral Nerve Injury Modulates Neurotrophin Signaling in the Peripheral and Central Nervous System. Mol Neurobiol *50*, 945–970.

Riss, T.L., Moravec, R.A., Niles, A.L., Duellman, S., Benink, H.A., Worzella, T.J., and Minor, L. (2004). Cell Viability Assays. In Assay Guidance Manual, S. Markossian, G.S.

Sittampalam, A. Grossman, K. Brimacombe, M. Arkin, D. Auld, C.P. Austin, J. Baell, J.M.M. Caaveiro, T.D.Y. Chung, et al., eds. (Bethesda (MD): Eli Lilly & Company and the National Center for Advancing Translational Sciences).

Rosano, G.L., and Ceccarelli, E.A. (2014). Recombinant protein expression in Escherichia coli: advances and challenges. Front Microbiol *5*.

Rotshenker, S. (2011). Wallerian degeneration: the innate-immune response to traumatic nerve injury. Journal of Neuroinflammation *8*, 109.

Saraste, A., and Pulkki, K. (2000). Morphologic and biochemical hallmarks of apoptosis. Cardiovasc Res *45*, 528–537.

Schwab, M.E., and Bartholdi, D. (1996). Degeneration and regeneration of axons in the lesioned spinal cord. Physiol Rev *76*, 319–370.

SEDDON, H.J. (1943). THREE TYPES OF NERVE INJURY. Brain *66*, 237–288.

Salehi, S., Koeck, K., and Scheibel, T. (2020). Spider Silk for Tissue Engineering Applications. Molecules *25*, 737.

Sierra, A., Tremblay, M.-È., and Wake, H. (2014). Never-resting microglia: physiological roles in the healthy brain and pathological implications. Front. Cell. Neurosci. *8*.

Simmons, J.R., Xu, L., and Rainey, J.K. (2019). Recombinant Pyriform Silk Fiber Mechanics Are Modulated by Wet-Spinning Conditions. ACS Biomater. Sci. Eng. *5*, 4985–4993.

Shypitsyna, A., Málaga-Trillo, E., Reuter, A., and Stuermer, C.A.O. (2011). Origin of Nogo-A by Domain Shuffling in an Early Jawed Vertebrate. Molecular Biology and Evolution *28*, 1363–1370.

Smeal, R.M., Rabbitt, R., Biran, R., and Tresco, P.A. (2005). Substrate curvature influences the direction of nerve outgrowth. Ann Biomed Eng *33*, 376–382.

Song, S., Wang, X., Wang, T., Yu, Q., Hou, Z., Zhu, Z., and Li, R. (2020). Additive Manufacturing of Nerve Guidance Conduits for Regeneration of Injured Peripheral Nerves. Front. Bioeng. Biotechnol. *8*.

Spieß, K., Wohlrab, S., and Scheibel, T. (2010). Structural characterization and functionalization of engineered spider silk films. Soft Matter *6*, 4168–4174.

Spiess, K., Ene, R., D. Keenan, C., Senker, J., Kremer, F., and Scheibel, T. (2011). Impact of initial solvent on thermal stability and mechanical properties of recombinant spider silk films. Journal of Materials Chemistry *21*, 13594–13604.

Straley, K.S., Foo, C.W.P., and Heilshorn, S.C. (2010). Biomaterial design strategies for the treatment of spinal cord injuries. J Neurotrauma *27*, 1–19.

Sutherland, T.D., Young, J.H., Weisman, S., Hayashi, C.Y., and Merritt, D.J. (2010). Insect silk: one name, many materials. Annu Rev Entomol *55*, 171–188.

Szeberényi, J., Cai, H., and Cooper, G.M. (1990). Effect of a dominant inhibitory Ha-ras mutation on neuronal differentiation of PC12 cells. Mol Cell Biol *10*, 5324–5332.

Tam, R.Y., Cooke, M.J., and Shoichet, M.S. (2012). A covalently modified hydrogel blend of hyaluronan–methyl cellulose with peptides and growth factors influences neural stem/progenitor cell fate. J. Mater. Chem. *22*, 19402–19411.

Terada, K., Kojima, Y., Watanabe, T., Izumo, N., Chiba, K., and Karube, Y. (2014). Inhibition of Nerve Growth Factor-Induced Neurite Outgrowth from PC12 Cells by Dexamethasone: Signaling Pathways through the Glucocorticoid Receptor and Phosphorylated Akt and ERK1/2. PLOS ONE *9*, e93223.

Tsuruma, A., Tanaka, M., Yamamoto, S., Fukushima, N., Yabu, H., and Shimomura, M. (2006). Topographical control of neurite extension on stripe-patterned polymer films. Colloids and Surfaces A: Physicochemical and Engineering Aspects *284–285*, 470–474.

Tucker, C.L., Jones, J.A., Bringhurst, H.N., Copeland, C.G., Addison, J.B., Weber, W.S., Mou, Q., Yarger, J.L., and Lewis, R.V. (2014). Mechanical and Physical Properties of Recombinant Spider Silk Films Using Organic and Aqueous Solvents. Biomacromolecules *15*, 3158–3170.

Waller, A.V., and Owen, R. (1850). XX. Experiments on the section of the glossopharyngeal and hypoglossal nerves of the frog, and observations of the alterations produced thereby in the structure of their primitive fibres. Philosophical Transactions of the Royal Society of London *140*, 423–429.

Wang, Z., Wang, Z., Lu, W.W., Zhen, W., Yang, D., and Peng, S. (2017). Novel biomaterial strategies for controlled growth factor delivery for biomedical applications. NPG Asia Mater *9*, e435–e435.

Watson, F.L., Heerssen, H.M., Moheban, D.B., Lin, M.Z., Sauvageot, C.M., Bhattacharyya, A., Pomeroy, S.L., and Segal, R.A. (1999). Rapid Nuclear Responses to Target-Derived Neurotrophins Require Retrograde Transport of Ligand–Receptor Complex. J. Neurosci. *19*, 7889–7900.

Weatherbee-Martin, N., Xu, L., Hupe, A., Kreplak, L., Fudge, D.S., Liu, X.-Q., and Rainey, J.K. (2016). Identification of Wet-Spinning and Post-Spin Stretching Methods Amenable to Recombinant Spider Aciniform Silk. Biomacromolecules *17*, 2737–2746.

Weinberg, H.J., and Spencer, P.S. (1978). The fate of Schwann cells isolated from axonal contact. J Neurocytol *7*, 555–569.

Wiatrak, B., Kubis-Kubiak, A., Piwowar, A., and Barg, E. (2020). PC12 Cell Line: Cell Types, Coating of Culture Vessels, Differentiation and Other Culture Conditions. Cells *9*, 958.

Wiesmann, C., Ultsch, M.H., Bass, S.H., and de Vos, A.M. (1999). Crystal structure of nerve growth factor in complex with the ligand-binding domain of the TrkA receptor. Nature *401*, 184–188.

Wong, W.T. (2013). Microglial aging in the healthy CNS: phenotypes, drivers, and rejuvenation. Front. Cell. Neurosci. *7*.

Xia, X.-X., Qian, Z.-G., Ki, C.S., Park, Y.H., Kaplan, D.L., and Lee, S.Y. (2010). Native-sized recombinant spider silk protein produced in metabolically engineered Escherichia coli results in a strong fiber. PNAS *107*, 14059–14063.

Xu, F., Na, L., Li, Y., and Chen, L. (2020). Roles of the PI3K/AKT/mTOR signalling pathways in neurodegenerative diseases and tumours. Cell & Bioscience *10*, 54.

Xu, L., Rainey, J.K., Meng, Q., and Liu, X.-Q. (2012a). Recombinant Minimalist Spider Wrapping Silk Proteins Capable of Native-Like Fiber Formation. PLOS ONE *7*, e50227.

Xu, L., Tremblay, M.-L., Meng, Q., Liu, X.-Q., and Rainey, J.K. (2012b). 1H, 13C and 15N NMR assignments of the aciniform spidroin (AcSp1) repetitive domain of Argiope trifasciata wrapping silk. Biomol NMR Assign *6*, 147–151.

Xu, L., Lefèvre, T., Orrell, K.E., Meng, Q., Auger, M., Liu, X.-Q., and Rainey, J.K. (2017). Structural and Mechanical Roles for the C-Terminal Nonrepetitive Domain Become Apparent in Recombinant Spider Aciniform Silk. Biomacromolecules *18*, 3678–3686.

Xu, L., Weatherbee-Martin, N., Liu, X.-Q., and Rainey, J.K. (2019). Recombinant Silk Fiber Properties Correlate to Prefibrillar Self-Assembly. Small *15*, 1805294.

Yan, Z., Li, Q., and Zhang, P. (2017). Soy Protein Isolate and Glycerol Hydrogen Bonding Using Two-Dimensional Correlation (2D-COS) Attenuated Total Reflection Fourier Transform Infrared (ATR FT-IR) Spectroscopy. Appl Spectrosc *71*, 2437–2445.

Yiu, G., and He, Z. (2006). Glial inhibition of CNS axon regeneration. Nat Rev Neurosci *7*, 617–627.

Young, S.L., Gupta, M., Hanske, C., Fery, A., Scheibel, T., and Tsukruk, V.V. (2012). Utilizing Conformational Changes for Patterning Thin Films of Recombinant Spider Silk Proteins. Biomacromolecules *13*, 3189–3199

Appendix: Supplementary Data

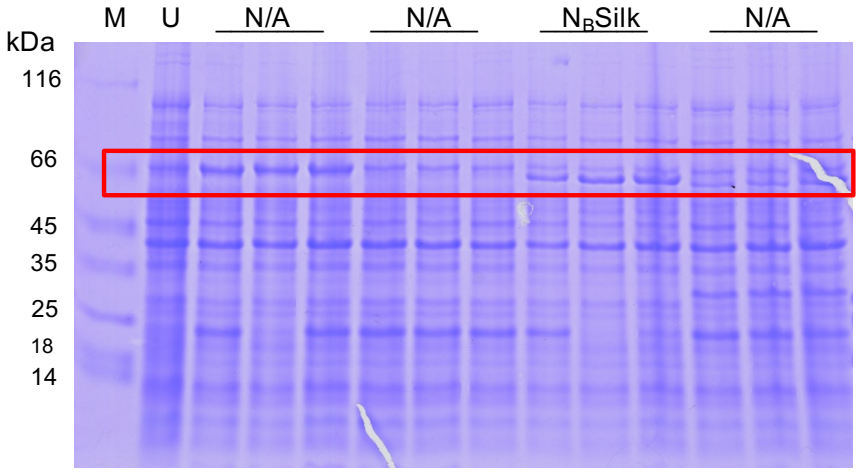

Figure A.1: Full SDS-PAGE Gel From Initial Test IPTG-Induced Expression of N_BSilk in Rosetta E. coli Cells. Following IPTG induction, cells were boiled to release their contents and the lysates were resolved by SDS-PAGE (Coomassie Blue stained) to check for the expression of N_BSilk. The induced N_BSilk samples (analyzed in triplicate) were compared to a cell lysate from uninduced cells (U). The red box highlights the expected electrophoretic mobility of N_BSilk at 55 kDa and shows the additional protein band present from overexpression. Lanes labelled N/A were other protein samples not relevant to N_BSilk studies. The image of Figure 2.3 was cropped from this gel.

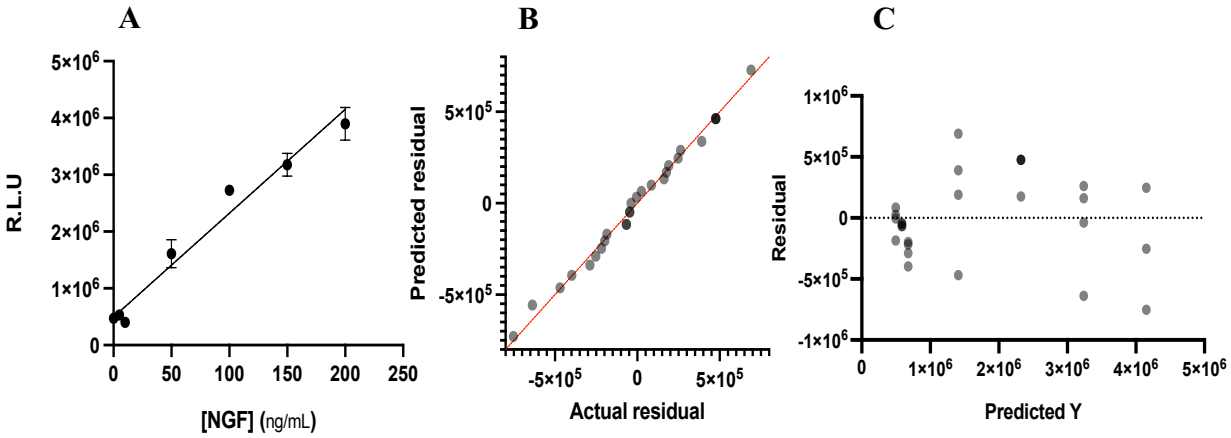

Figure A.2: NGF-Binding ELISA Assay Validation. A) ELISA standard graph of human NGF-β primary antibody against NGF-β on non-treated 96-well plates to show the affinity of the antibody is dependent on the concentration of NGF- β. The relationship between R.L.U as a function of NGF concentration was fit based on the standard curve. A QQ plot **(B)** and the residuals **(C)** were plotted to further analyse the relationship between NGF and the primary antibody.

Table A.1: P-Values from PC12 Adh Neurite Density Analysis on Day 7 of Cell Culture.

Tukey's multiple comparisons test	Summary	Adjusted P Value
Plate vs. Plate+ NGF-M	*	0.0123
Plate vs. Silk	ns	0.9713
Plate vs. Silk+ NGF-M	*	0.0111
Plate vs. Silk+ NGF-L	****	<0.0001
Plate vs. Silk+ NGF-M, NGF-L	****	<0.0001
Plate+ NGF-M vs. Silk	ns	0.0576
Plate+ NGF-M vs. Silk+ NGF-M	ns	>0.9999
Plate+ NGF-M vs. Silk+ NGF-L	***	0.0004
Plate+ NGF-M vs. Silk+ NGF-M, NGF-L	*	0.0172
Silk vs. Silk+ NGF-M	ns	0.0526
Silk vs. Silk+ NGF-L	****	<0.0001
Silk vs. Silk+ NGF-M, NGF-L	****	<0.0001
Silk+ NGF-M vs. Silk+ NGF-L	***	0.0004
Silk+ NGF-M vs. Silk+ NGF-M, NGF-L	*	0.0189
Silk+ NGF-L vs. Silk+ NGF-M, NGF-L	ns	0.4891

* = p-value < 0.05. ** = p-value < 0.005. *** = p-value < 0.0005. **** = p-value < 0.0001. Non-significant findings are labelled “ns”. P-values in addition to those shown in Figure 3.5 A.

Table A.2: P-Values from PC12 Adh Neurite Length Analysis on Day 7 of Cell Culture.

Tukey's multiple comparisons test	Summary	Adjusted P Value
Plate vs. Plate+	*	0.0228
Plate vs. Silk	ns	0.9600
Plate vs. Silk+	**	0.0086
Plate vs. Preloaded Silk	*	0.0437
Plate vs. Preloaded Silk+	*	0.0379
Plate+ vs. Silk	ns	0.1136
Plate+ vs. Silk+	ns	0.9968
Plate+ vs. Preloaded Silk	ns	0.9995
Plate+ vs. Preloaded Silk+	ns	0.9998
Silk vs. Silk+	*	0.0466
Silk vs. Preloaded Silk	ns	0.1991
Silk vs. Preloaded Silk+	ns	0.1768
Silk+ vs. Preloaded Silk	ns	0.9662
Silk+ vs. Preloaded Silk+	ns	0.9774
Preloaded Silk vs. Preloaded Silk+	ns	>0.9999

* = p-value < 0.05. ** = p-value < 0.005. Non-significant findings are labelled “ns”. P-values in addition to those shown in Figure 3.5 B.

Table A.3: **P-values from the Western Blot Analysis of pERK/ERK in PC12 Cells.**

Tukey's multiple comparisons test	Summary	Adjusted P Value
Col 1 vs. Col 1+ NGF-M	*	0.0239
Col 1 vs. Col 4	ns	>0.9999
Col 1 vs. Col 4+ NGF-M	*	0.0245
Col 1 vs. Silk	ns	0.9405
Col 1 vs. Silk+ NGF-M	*	0.0334
Col 1 vs. Silk+ NGF-L	**	0.0052
Col 1 vs. Silk+ NGF-M, NGF-L	**	0.0026
Col 1+ NGF-M vs. Col 4	*	0.0499
Col 1+ NGF-M vs. Col 4+ NGF-M	ns	>0.9999
Col 1+ NGF-M vs. Silk	ns	0.1856
Col 1+ NGF-M vs. Silk+ NGF-M	ns	>0.9999
Col 1+ NGF-M vs. Silk-NGF-L	ns	0.9914
Col 1+NGF-M vs. Silk+ NGF-M, NGF-L	ns	0.9362
Col 4 vs. Col 4+ NGF-M	ns	0.0510
Col 4 vs. Silk	ns	0.9940
Col 4 vs. Silk+ NGF-M	ns	0.0690
Col 4 vs. Silk+ NGF-L	*	0.0110
Col 4 vs. Silk+ NGF-M, NGF-L	**	0.0055
Col 4+ NGF-M vs. Silk	ns	0.1891
Col 4+ NGF-M vs. Silk+ NGF-M	ns	>0.9999
Col 4+ NGF-M vs. Silk+ NGF-L	ns	0.9906
Col 4+ NGF-M vs. Silk+ NGF-M, NGF-L	ns	0.9331
Silk vs. Silk+ NGF-M	ns	0.2444
Silk vs. Silk+ NGF-L	*	0.0458
Silk vs. Silk+ NGF-M, NGF-L	*	0.0232
Silk+ NGF-M vs. Silk+ NGF-L	ns	0.9737
Silk+ NGF-M vs. Silk+ NGF-M, NGF-L	ns	0.8786
Silk+ NGF-L vs. Silk+ NGF-M, NGF-L	ns	>0.9999

* = p-value < 0.05. ** = p-value < 0.005. Non-significant findings are labelled “ns”. P-values in addition to those shown in Figure 3.6 A.

Table A.4: P-values from the Western Blot Analysis of pAKT/AKT in PC12 Cells.

Tukey's multiple comparisons test	Summary	Adjusted P Value
Col 1 vs. Col 1+ NGF-M	***	0.0002
Col 1 vs. Col 4	ns	0.9906
Col 1 vs. Col 4+ NGF-M	**	0.0015
Col 1 vs. Silk	ns	0.5157
Col 1 vs. Silk+ NGF-M	*	0.0143
Col 1 vs. Silk+ NGF-L	**	0.0029
Col 1 vs. Silk+ NGF-M, NGF-L	***	0.0005
Col 1+ NGF-M vs. Col 4	***	0.0010
Col 1+ NGF-M vs. Col 4+ NGF-M	ns	0.9607
Col 1+ NGF-M vs. Silk	**	0.0095
Col 1+ NGF-M vs. Silk+ NGF-M	ns	0.3978
Col 1+ NGF-M vs. Silk-NGF-L	ns	0.8501
Col 1+NGF-M vs. Silk+ NGF-M, NGF-L	ns	0.9996
Col 4 vs. Col 4+ NGF-M	**	0.0070
Col 4 vs. Silk	ns	0.9236
Col 4 vs. Silk+ NGF-M	ns	0.0660
Col 4 vs. Silk+ NGF-L	*	0.0139
Col 4 vs. Silk+ NGF-M, NGF-L	**	0.0024
Col 4+ NGF-M vs. Silk	ns	0.0690
Col 4+ NGF-M vs. Silk+ NGF-M	ns	0.9307
Col 4+ NGF-M vs. Silk+ NGF-L	ns	>0.9999
Col 4+ NGF-M vs. Silk+ NGF-M, NGF-L	ns	0.9989
Silk vs. Silk+ NGF-M	ns	0.4415
Silk vs. Silk+ NGF-L	ns	0.1285
Silk vs. Silk+ NGF-M, NGF-L	*	0.0240
Silk+ NGF-M vs. Silk+ NGF-L	ns	0.9895
Silk+ NGF-M vs. Silk+ NGF-M, NGF-L	ns	0.6725
Silk+ NGF-L vs. Silk+ NGF-M, NGF-L	ns	0.9807

* = p-value < 0.05. ** = p-value < 0.005. *** = p-value < 0.0005. Non-significant findings are labelled “ns”. P-values in addition to those shown in Figure 3.6 B.

Table A.5: P-values from the Western Blot Analysis of pERK/ERK in PC12 Adh Cells.

Tukey's multiple comparisons test	Summary	Adjusted P Value
Plate vs. Plate+ NGF-M	ns	0.0704
Plate vs. Silk	ns	0.7593
Plate vs. Silk+ NGF-M	*	0.0344
Plate vs. Silk+ NGF-L	ns	0.0838
Plate vs. Silk+ NGF-M, NGF-L	*	0.0113
Plate+ NGF-M vs. Silk	ns	0.4927
Plate+ NGF-M vs. Silk+ NGF-M	ns	0.9977
Plate+ NGF-M vs. Silk+ NGF-L	ns	>0.9999
Plate+ NGF-M vs. Silk+ NGF-M, NGF-L	ns	0.8772
Silk vs. Silk+ NGF-M	ns	0.2881
Silk vs. Silk+ NGF-L	ns	0.5514
Silk vs. Silk+ NGF-M, NGF-L	ns	0.1063
Silk+ NGF-M vs. Silk+ NGF-L	ns	0.9936
Silk+ NGF-M vs. Silk+ NGF-M, NGF-L	ns	0.9832
Silk+ NGF-L vs. Silk+ NGF-M, NGF-L	ns	0.8321

* = p-value < 0.05. Non-significant findings are labelled “ns”. P-values in addition to those shown in Figure 3.7 A.

Table A.6: P-values from the Western Blot Analysis of pAKT/AKT in PC12 Adh Cells.

Tukey's multiple comparisons test	Summary	Adjusted P Value
Plate vs. Plate+ NGF-M	ns	0.9331
Plate vs. Silk	ns	0.9990
Plate vs. Silk+ NGF-M	ns	0.9992
Plate vs. Silk+ NGF-L	ns	0.5621
Plate vs. Silk+ NGF-M, NGF-L	ns	0.1042
Plate+ NGF-M vs. Silk	ns	0.9919
Plate+ NGF-M vs. Silk+ NGF-M	ns	0.9908
Plate+ NGF-M vs. Silk+ NGF-L	ns	0.9682
Plate+ NGF-M vs. Silk+ NGF-M, NGF-L	ns	0.4000
Silk vs. Silk+ NGF-M	ns	>0.9999
Silk vs. Silk+ NGF-L	ns	0.7656
Silk vs. Silk+ NGF-M, NGF-L	ns	0.1837
Silk+ NGF-M vs. Silk+ NGF-L	ns	0.7569
Silk+ NGF-M vs. Silk+ NGF-M, NGF-L	ns	0.1791
Silk+ NGF-L vs. Silk+ NGF-M, NGF-L	ns	0.8176

Non-significant findings are labelled “ns”. P-values in addition to those shown in Figure 3.7 B.